diversity

MDPI

Article

Empirically Calibrated Phytoindication Scales Resolve Complementary Edaphic and Topographic Components of the Moisture Regime

Hanna Tutova [1], Olena Lisovets [2], Olha Kunakh [2] and Olexander Zhukov [1,*]

[1] Department of Botany, Ecology and Horticulture, Bogdan Khmelnytskyi Melitopol State Pedagogical University, 72300 Zaporizhzhia, Ukraine; annatutova37@gmail.com
[2] Department of Biodiversity and Ecology, Oles Honchar Dnipro National University, Gagarin Avenue, 72, 49000 Dnipro, Ukraine; lisovetselena@gmail.com (O.L.); kunah_olga@ukr.net (O.K.)
* Correspondence: zhukov_dnipro@ukr.net

Abstract

The moisture regime is one of the principal determinants of plant distribution; however, traditional phytoindication systems generally treat it as a single ecological gradient, despite its complex environmental controls. This study examined whether vegetation responses could be used to integrate climatic, edaphic, and topographic determinants of moisture availability into ecologically meaningful indicator scales. European GBIF occurrence records for the regional flora were combined with climatic, edaphic, and topographic predictors, and the resulting moisture indicators were evaluated using vegetation plots, Sentinel-2 NDWI data, field soil-moisture measurements, and permutation-based null-model analyses. Constrained canonical correspondence analysis, using annual precipitation, topographic wetness index (TWI), and soil texture as environmental predictors, identified complementary moisture components that were used to derive empirically calibrated Edaphic Moisture Index (EMI) and Topographic Moisture Index (TMI). The edaphic component explained 32.7% of constrained variation and showed strong agreement with traditional moisture scales (R^2 = 0.75–0.80), whereas the topographic component explained an additional 24.1% of constrained variation and represented a complementary dimension of moisture variation. Species-level EMI and TMI values were subsequently evaluated in relation to traditional Didukh and Ellenberg phytoindication systems using multiple complementary approaches, including vegetation plot analyses, landscape-scale assessment of spatial agreement with environmental moisture gradients, and permutation-based null-model testing. Both EMI and TMI captured vegetation-associated moisture variation and enabled spatial characterization of moisture conditions, although improvements over traditional indicators were scale-dependent rather than universally greater. These findings indicate that vegetation-based moisture assessment benefits from considering complementary edaphic and topographic components of the moisture regime rather than representing moisture conditions as a single undifferentiated gradient. The framework extends traditional phytoindication by providing empirically calibrated indicators that integrate vegetation responses with environmental predictors for ecological assessment.

Keywords: phytoindication; Edaphic Moisture Index (EMI); Topographic Moisture Index (TMI); indicator value calibration; GBIF occurrence records

Check for updates

Academic Editor: Giovanni Bacaro

Received: 27 June 2026
Revised: 19 August 2026
Accepted: 21 August 2026
Published: 25 August 2026

Copyright: © 2026 by the authors. Licensee MDPI, Basel, Switzerland. This article is an open access article distributed under the terms and conditions of the Creative Commons Attribution (CC BY) license.

1. Introduction

The moisture regime of a terrestrial habitat may be defined as the recurring temporal dynamics of soil water availability [1,2]. The degree of congruence between these and the ecological requirements of living organisms determines the suitability of environmental conditions for plant communities, as well as for associated assemblages of animals and microorganisms [3,4]. Congruence should be understood both as the correspondence between water availability and the requirements of organisms, and as the mutual adjustment of abiotic and biotic processes that together shape the moisture regime itself [5]. Abiotic controls of the moisture regime include precipitation, evaporative demand, relief, soil susceptibility to erosion, groundwater level, and other physical drivers of water input, redistribution, storage, and loss [6]. In turn, biotic controls include evapotranspiration by vegetation, the protective effect of plant cover against erosion [7], the accumulation of organic matter, which increases soil stability and water retention, and the biologically mediated formation of soil porosity and structure, which redirects pathways for infiltration, redistribution, and storage of water [8–10]. Thus, congruence reflects a reciprocal relationship: abiotic conditions constrain living organisms, while organisms and their communities modify the same conditions through their effects on soil structure, erosion resistance, organic matter accumulation, and water fluxes. The ecological moisture regime results from interactions among multiple environmental controls, including climatic water supply, soil properties affecting water retention, and topographic processes regulating water redistribution. These components operate through partly independent mechanisms and are characterized by different spatial scales, yet their integrated effects are expressed in vegetation patterns [11,12].

In ecology, the moisture regime as an ecological factor is commonly represented by two main approaches: phytoindication [13–15] and climatic moisture coefficients. The latter are based on combinations of climatic variables, most commonly precipitation and potential evapotranspiration, which are assumed to determine plant water availability [16]. Phytoindication infers environmental conditions from the composition of plant communities and is based on the ecological preferences of plant species along moisture gradients [17]. In this approach, species indicator values are interpreted as biologically integrated responses to the combined action of environmental factors [18]. By contrast, climatic moisture coefficients represent the moisture regime as combinations of measured environmental variables, such as precipitation, temperature, evapotranspiration, and other parameters assumed to determine water availability for plants [19].

Phytoindication systems enable the assessment of ecological conditions from the species composition of plant communities, thereby integrating information on the climatic, edaphic, hydrological, and topographic components of the water regime [20]. The best-known examples are Ellenberg's modal indicator values, which characterise the position of species' ecological optima along a moisture gradient [21], and Didukh's range-based phytoindication system, which describes species' tolerance limits with respect to water regime conditions [14,22]. Both approaches have been successfully applied to the assessment of ecological conditions in vegetation [20,23]. However, they reflect the integrated outcome of multiple interacting factors and do not allow the direct disentanglement of the contributions of individual mechanisms governing the moisture regime [18]. Classical phytoindication approaches should be noted as being based on the expert synthesis of species' ecological behaviour. Numerous studies have demonstrated substantial agreement between phytoindication-based assessments of moisture conditions and independently measured or modelled characteristics of the water regime. Such relationships have been established for climatic moisture indices [24,25], soil moisture [17,26,27], groundwater levels [26,28], topographically driven moisture accumulation [29–32], and remote-sensing

indices sensitive to vegetation or land-surface water status [33–35]. Phytoindication scales may be regarded as empirically validated, integrative assessments of the water regime, reflecting an ecologically meaningful combination of climatic, edaphic, hydrological, and topographic conditions relevant to plants.

European-scale syntheses have focused primarily on harmonizing existing expert-derived ecological indicator systems. Trans-European Ellenberg-type indicator values have been obtained through the integration of regional indicator systems and, where necessary, statistical completion based on species co-occurrence patterns in large European vegetation databases [21]. Approaches integrating multiple expert-based assessments have enabled the transformation of heterogeneous indicator systems into common continuous scales and the estimation of species niche breadth in addition to ecological optima [36]. Evaluations of plant indicator values have relied on vegetation plot datasets and comparisons with measured environmental variables, mostly at local or landscape scales. Such approaches have provided important assessments of the reliability of expert-derived indicator values by comparing species-based estimates with independently measured environmental conditions [20,31]. Berg et al. [37] revised Ellenberg's continentality values by using standardized information on global species distributions and converting species range patterns into quantitative continentality scores. However, these values represent biogeographic characteristics of species distributions rather than direct estimates calibrated against measured environmental variables. Large-scale occurrence databases provide opportunities to characterize species–environment relationships across broad environmental gradients and offer a potential basis for empirically deriving plant indicator values. GBIF-based occurrence data have been demonstrated to provide reliable estimates of species' climate niche properties when uneven sampling effort is accounted for [38]. Applying occurrence data for the derivation and calibration of ecological indicators requires addressing methodological challenges, including spatial sampling bias, uneven environmental representation, and the need for appropriate strategies for data aggregation and validation.

Phytoindication reflects the realised ecological response of vegetation, whereas climatic moisture coefficients provide a physically based reconstruction of the environmental conditions shaping plant habitats. Both approaches offer complementary frameworks for representing the moisture regime as an ecological factor [11,39]. Despite their successful application, an important conceptual gap remains: traditional phytoindication systems generally represent moisture conditions as integrated one-dimensional gradients and do not allow separation of the distinct environmental mechanisms underlying moisture availability, particularly soil water retention and topographically driven water redistribution. Resolving this limitation requires approaches that use botanical data to disentangle complementary components of the moisture regime and clarify the ecological meaning of plant-based moisture indicators.

The steppe zone of southeastern Ukraine provides an appropriate natural laboratory for disentangling complementary components of the moisture regime. This region encompasses pronounced gradients in climatic water availability [40,41], soil properties [42,43], and topographic conditions [44], resulting in high environmental heterogeneity and a floristically diverse vegetation cover that includes species with contrasting ecological moisture preferences [45–47]. The regional flora is supported by comprehensive ecological information, including European-scale Ellenberg indicator values [21,36], the national Didukh phytoindication system [14], and regional ecological characteristics compiled by Tarasov [48], providing an independent basis for calibration and evaluation of moisture indicator values.

This study aimed to identify a principled approach for separating complementary components of the moisture regime using vegetation responses as an integrative ecological

signal. Specifically, the study pursued three objectives: (1) to elucidate the multidimensional structure of vegetation responses to moisture-related environmental gradients represented by precipitation, topographic wetness index (TWI), and soil texture; (2) to derive empirically based Edaphic Moisture Index (EMI) and Topographic Moisture Index (TMI) as spatially explicit indicators of complementary moisture components; and (3) to evaluate the ecological meaning and spatial consistency of these indicators in comparison with traditional phytoindication systems using vegetation datasets and environmental moisture gradients. The study represents a regional case study based on the flora and landscapes of southeastern Ukraine, intended to test the methodological framework rather than provide a continental-scale moisture mapping system or climate-change projection tool. Specifically, this study addressed the following scientific questions: (1) How are vegetation responses to moisture availability structured by precipitation, topographic wetness index (TWI), and soil texture, and can distinct moisture-related components be identified? (2) How can an ecologically meaningful metric of plant moisture availability be derived from abiotic environmental predictors and vegetation responses? (3) Which components of the moisture regime are captured by traditional phytoindication systems, and which components remain unresolved? The proposed framework was evaluated through a hierarchical assessment framework, including European-scale occurrence-data modelling for indicator derivation, regional-scale assessment using vegetation plot datasets, and landscape-scale evaluation of spatial agreement with environmental moisture gradients based on remote-sensing moisture proxies (NDWI), field observations, and null-model analyses. The study provides both conceptual and methodological advances. Conceptually, it moves beyond the representation of moisture conditions as a single integrated ecological gradient by distinguishing complementary edaphic and topographic components of the moisture regime and clarifying their relationships with vegetation responses. Methodologically, it develops spatially explicit moisture indicators that integrate vegetation-based information with environmental predictors and can serve as a framework for ecological assessment across comparable environmental contexts.

2. Materials and Methods

2.1. Conceptual Framework

The study was based on the premise that precipitation, Topographic Wetness Index (TWI), and soil texture represent complementary abiotic markers of the water regime (Figure 1). Their ecological significance was assessed through the structure of species distributions, which was treated as the realised plant species response to the combined action of these environmental controls. At the community level, this response was interpreted as an integrative signal reflecting both the influence of abiotic moisture-regulating factors and the plant community's role as a modulator of the moisture regime through its effects on evapotranspiration, soil protection, organic matter accumulation, soil structure, and water redistribution.

The case study was conducted using the regional flora of the steppe zone of southeastern Ukraine as a model system to analyse relationships between species distributions and abiotic markers of the water regime. The study area encompasses pronounced environmental gradients associated with climatic, edaphic, geomorphological, and vegetation heterogeneity. The climatic conditions are characterized by a precipitation gradient typical of the Ukrainian steppe zone, with mean annual precipitation increasing from approximately 350 mm in the southern and southeastern parts to 500–550 mm in the northwestern direction, resulting in substantial spatial variation in water availability. Soil diversity reflects the interaction between relief and hydrological conditions: chernozems dominate on relatively elevated watershed positions and ravine slopes, meadow and

wetland soils occur in floodplains, whereas sandy soils are characteristic of the first above-floodplain terraces (Psammophytic steppe). The landscape is predominantly composed of plains dissected by ravine–gully systems and river valleys, which regulate local redistribution of surface and subsurface moisture. These environmental gradients are associated with distinct vegetation patterns: steppe communities dominate on zonal upland sites, meadow and forest communities occur in ravines, while floodplains and above-floodplain terraces support a mosaic of forests, wetlands, meadows, and saline vegetation.

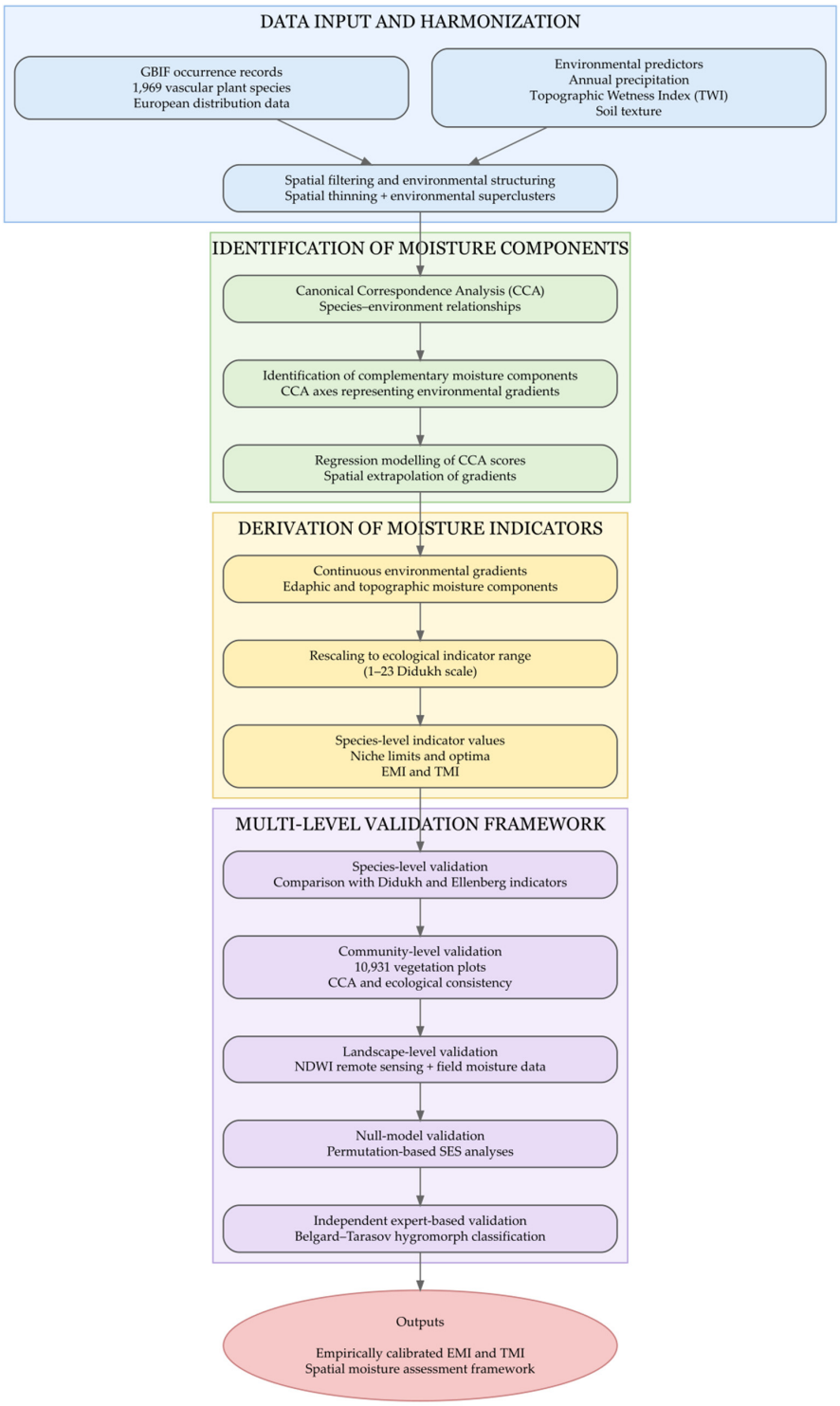


Figure 1. Conceptual workflow for the derivation and assessment of empirically calibrated moisture indicators (EMI and TMI). The framework integrates European-scale species occurrence data from GBIF

with environmental predictors (annual precipitation, topographic wetness index, and soil texture), followed by spatial thinning and environmental stratification. Canonical correspondence analysis (CCA) is used to identify complementary moisture components, which are transformed into species-level Edaphic Moisture Index (EMI) and Topographic Moisture Index (TMI) values. The resulting indicators are evaluated through a hierarchical assessment framework, including species-level comparisons with traditional phytoindication systems, community-level assessment using vegetation plots, landscape-scale assessment of spatial agreement with NDWI remote-sensing data and field moisture measurements, permutation-based null-model testing, and expert-based classification.

The target species pool comprised vascular plant species included in the flora of the Dnipropetrovsk and Zaporizhzhia regions of Ukraine (Figure 2). The regional flora served only as the pool of calibration species. Species-specific moisture coefficients were estimated using the complete European occurrence records of each species available through GBIF rather than their occurrences within Ukraine alone. Because the regional flora encompasses species spanning the full European moisture gradient, from xerophytic to hygrophytic taxa, it provides an appropriate basis for calibration.

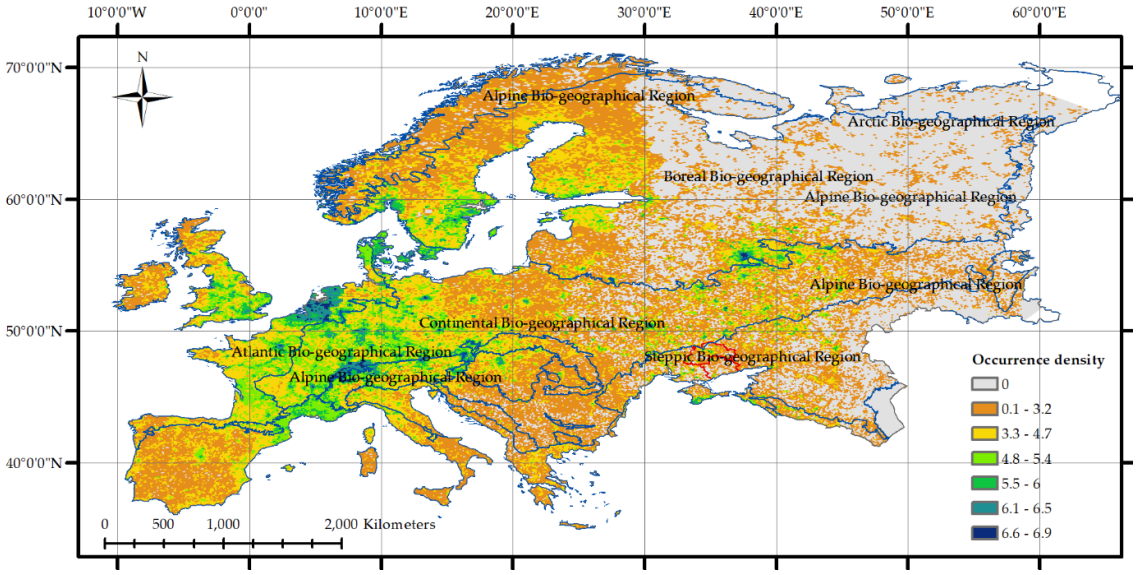


Figure 2. Spatial distribution across Europe of GBIF occurrence records for plant species comprising the reference species pool of the Dnipropetrovsk and Zaporizhzhia regions of Ukraine. Colours indicate the logarithmically transformed density of unique occurrences, log10(1 + number of occurrences). Major European biogeographical regions are shown for reference. The red outline indicates the reference region in southeastern Ukraine.

This flora is well documented and supported by extensive ecological information, including Ellenberg moisture indicator values [23], Didukh's range-based phytoindication estimates [25], and the Belgard–Tarasov hygromorph classification [47], an additional expert-based source of information on species moisture preferences. This combination of floristic, distributional, and ecological data enabled evaluation of how abiotic moisture-related markers are expressed in species distributions and how the resulting botanical response relates to established phytoindication systems. As the primary reference, the comprehensive floristic and ecological synthesis by Tarasov [48] was used, which provides ecological characteristics for vascular plant species occurring in the Dnipropetrovsk and Zaporizhzhia regions.

The original compilation included 2027 vascular plant species. Additional floristic information collected during subsequent studies expanded the checklist to 2131 species.

Species were classified as cultivated, agricultural, or ornamental according to the floristic synopsis of Tarasov [48], which identifies taxa occurring exclusively in cultivation. After taxonomic harmonisation and synonym matching, exclusion of cultivated agricultural and ornamental species, and removal of taxa represented by fewer than 10 occurrence records, the final species pool comprised 1963 vascular plant species. This regional flora is particularly suitable for developing moisture indicator systems because it combines species occurrence data with several independent ecological classifications that describe plant responses to water availability. The database contains Ellenberg moisture indicator values [13,36], which characterise the ecological optimum of species along the moisture gradient, and Didukh moisture indicator values [14], which describe the lower and upper limits of favourable moisture conditions. In addition, the compilation includes Belgard–Tarasov hygromorph categories, an expert-based ordinal classification of plant species according to their moisture preferences [48]. The coexistence of continuous indicator scales (Ellenberg and Didukh) and an independent ordinal hygromorph classification provides an opportunity to construct and assess new moisture indicator systems. The traditional phytoindication scales were used as ecological references for calibration of occurrence-derived moisture estimates, whereas the Belgard–Tarasov hygromorph classification served as an independent source of ecological information for subsequent assessment of spatial and ecological consistency. This framework allowed assessment of whether the newly developed moisture scales reproduce established ecological knowledge while also capturing additional dimensions of moisture variability not represented in traditional indicator systems.

Georeferenced occurrence records of all species included in the regional flora were compiled from the GBIF database across Europe to capture this integrated response [49,50]. This broad geographic coverage ensured that species responses were evaluated across a much wider range of environmental conditions than those available within the reference region alone. For each occurrence record, annual precipitation, topographic wetness index (TWI), and soil texture characteristics were extracted. Occurrence records were then aggregated to the species level, yielding a species-by-environment matrix describing the distribution of species across combinations of potential moisture-regulating environmental conditions. This matrix was used to identify the principal patterns of floristic variation associated with the moisture-related predictors. The resulting floristic gradients were interpreted as integrated ecological responses to the combined effects of precipitation, topography, and soil properties. These gradients provided the basis for deriving two complementary moisture indicators. The first reflected variation, primarily associated with soil-mediated water availability, was interpreted as an edaphic moisture gradient. The second reflected variation, associated with topographically driven redistribution of water, was interpreted as a topographic moisture gradient. Subsequent analyses focused on calibrating these gradients as indicator scales and evaluating their ecological performance using independent vegetation datasets, remote-sensing proxies of moisture conditions, and expert-based ecological classifications.

2.2. European Occurrence Dataset for the Reference Flora

Species occurrence data were obtained from the Global Biodiversity Information Facility (GBIF; https://www.gbif.org, accessed on 15 June 2026) [49,50] using automated queries implemented through the RGBIF package in R [51]. All available georeferenced occurrence records for each species within Europe were retrieved and subsequently merged into a unified database. Occurrence records were subjected to quality control by removing records with missing or invalid geographic coordinates, including records located at country or administrative unit centroids or representing obviously generalized localities. Records

with reported coordinate uncertainty exceeding 500 m were excluded. Duplicate occurrences were removed after coordinate standardization, and records lacking environmental predictor values were excluded. Occurrence records explicitly identified as cultivated agricultural or ornamental observations were removed based on cultivation status information provided in the occurrence records.

The vegetation plot dataset used for subsequent community-level assessments (Section 2.8) was used to identify potential spatial overlap between the calibration and assessment datasets. This dataset comprised 10,931 relevés representing vascular plant community composition across the southeastern Ukrainian steppe zone. Species occurrences within relevés were converted into 123,929 species–plot observations, and geographic coordinates of the plots were assigned to the same 10 × 10 km grid system used for processing GBIF records. This resulted in 6556 unique species–grid combinations representing the spatial distribution of the assessment dataset. GBIF occurrence records were assigned to the same 10 × 10 km grid system, and records corresponding to the same species and grid cells represented in the assessment dataset were excluded before spatial thinning. This procedure removed 20,645 occurrence records and resulted in a calibration dataset containing 13,209,301 occurrence records. The remaining occurrence records were spatially thinned by retaining a single occurrence per species within each 10 × 10 km grid cell to reduce the influence of spatial sampling bias caused by uneven collecting effort and repeated observations. This procedure reduced the dataset to 4,676,517 unique species–grid records while preserving the broad-scale geographical structure of species distributions. Occurrence records were aggregated to a common 10 km grid to reduce the influence of spatially uneven sampling effort across Europe and to minimize bias associated with oversampled regions. The selected grid size also matches the spatial resolution of the precipitation data used in the analyses, ensuring consistency between biological observations and environmental predictors. Among the 1963 species-level taxa retained in the calibration dataset, 1791 taxa (91.2%) were represented by more than 100 records, whereas 95 taxa had 31–100 records and 77 taxa had 10–30 records. Across all taxa, the median number of occurrence records was 5855 (Q1–Q3: 626–11,930), with a maximum of 56,632 records per taxon. Although the species pool investigated originates from the flora of southeastern Ukraine, many of these species occur across a wide range of European biogeographical regions. Their continental-scale distributions provide a substantially broader environmental gradient than that available within the reference region alone, thereby enabling robust estimation of species–environment relationships.

2.3. Environmental Predictors Representing Climatic, Topographic, and Edaphic Controls of the Moisture Regime

Topographic wetness was represented by the Topographic Wetness Index (TWI) [52] derived from the Multiscale Land Surface Parameters of the Global Ensemble Digital Terrain Model (GEDTM30) [53]. The dataset provides global TWI layers at multiple spatial resolutions and is distributed as Cloud Optimised GeoTIFF files in EPSG:4326. In this study, the 240 m TWI layer was used as the topographic moisture predictor and was reprojected and resampled to the common European grid in ETRS89/LAEA Europe (EPSG:3035) with a 250 m spatial resolution. The TWI layer was used to characterise local topographic control on potential water accumulation and redistribution across the European distribution range of the analysed species.

Annual precipitation was derived from WorldClim version 2.1 monthly precipitation layers [54]. Annual precipitation was selected as a broad-scale climatic predictor because the objective of the study was to characterize continental-scale moisture gradients. Although seasonal precipitation patterns may further refine species-specific moisture relationships, annual precipitation provides a robust and spatially consistent climatic descriptor at the

European scale. Monthly precipitation data were obtained using the geodata package in R [55] at 0.5 arc-minute spatial resolution and cropped to the European study extent. The twelve monthly precipitation layers were summed to obtain annual precipitation. The resulting raster was reprojected and resampled to the common European grid in ETRS89/LAEA Europe (EPSG:3035) with a 250 m spatial resolution.

Soil texture was characterised using SoilGrids global predictions of sand and clay content for the 0–5 cm soil layer [56]. The corresponding raster layers were obtained through the geodata package in R, cropped to the European study extent, reprojected to ETRS89/LAEA Europe (EPSG:3035), and resampled to a common 250 m grid. Sand and clay contents were combined into a texture coefficient to represent the hydrological effect of soil texture by a single continuous variable. The sand-to-clay ratio was calculated and log-transformed. The resulting values were then converted using a sigmoid transformation:

$$\text{Texture} = \frac{1}{1 + \exp(ln\frac{\text{sand}+1}{\text{clay}+1})},$$

where higher values correspond to finer-textured, clay-rich soils with greater water-retention potential, whereas lower values indicate coarse-textured, sandy soils with higher permeability, this transformation yielded a dimensionless index ranging from 0 to 1 and was subsequently used as a predictor in all analyses. The 0–5 cm SoilGrids layer was used as a spatially consistent proxy for landscape-scale variation in soil texture rather than as a direct representation of the rooting environment of individual species. Because rooting depth varies substantially among vascular plants, selecting a deeper soil layer would not resolve this limitation, as no single depth can adequately represent the rooting environment of all species. Accordingly, the texture variable should be interpreted as a landscape-scale indicator of edaphic conditions rather than a direct measure of plant-available water for individual taxa.

2.4. Species–Environment Matrix Construction and Canonical Correspondence Analysis

A species matrix for multivariate analysis was constructed using individual species occurrence records for which environmental values were successfully extracted. Records with missing values for TWI, annual precipitation, soil texture coefficient, or species identity were excluded. The remaining records were classified according to their environmental position using three predictors: Topographic Wetness Index (TWI), annual precipitation, and the soil texture coefficient. TWI and annual precipitation were each divided into 15 quantile-based classes, whereas the soil texture coefficient was divided into 10 quantile-based classes. The combination of these three classes defined an environmental supercluster, representing a discrete unit of environmental space rather than a geographical grid cell. The combination of these environmental classes resulted in 2250 environmental superclusters ($15 \times 15 \times 10$), each representing a discrete unit of environmental space. A species-by-supercluster matrix, hereafter referred to as the species matrix, was then constructed by counting the number of occurrence records of each species within each environmental supercluster. Rows of the matrix corresponded to environmental superclusters, columns corresponded to species, and cell values represented the number of records of a given species in a given supercluster. Missing species–supercluster combinations were assigned a value of 0. The corresponding environmental matrix was obtained by calculating mean TWI, annual precipitation, and soil texture coefficient for each supercluster, together with the number of occurrence records assigned to it. This paired species–environmental matrix was subsequently used in a canonical correspondence analysis.

Species-specific moisture indicator values were linked to occurrence records before aggregation to facilitate the interpretation of ecological gradients identified by canonical cor-

respondence analysis. The corresponding Didukh minimum moisture value (Didukh_min), Didukh maximum moisture value (Didukh_max), and Ellenberg moisture indicator value (Ellenberg_F) were assigned based on species identity for each occurrence record. Subsequently, mean indicator values were calculated for each environmental stratum by averaging the indicator scores of all occurrence records assigned to that stratum. These aggregated indicator values were incorporated into the environmental matrix and used to characterise the ecological position of environmental strata along established phytoindication gradients of moisture availability.

Canonical correspondence analysis (CCA) [57] was used to relate species composition in environmental strata to the three environmental predictors. The species matrix, containing occurrence counts of each species within each environmental stratum, was used as the response matrix. Mean annual precipitation (P_mm), mean Topographic Wetness Index (TWI), and mean soil texture coefficient (texture_coef) calculated for the same strata were used as explanatory variables. The CCA model included all main effects and their interactions:

$$\text{species_matrix} \sim \text{P_mm} \times \text{TWI} \times \text{Texture}.$$

Thus, the ordination assessed the joint and interactive effects of climatic water supply, topographic moisture redistribution, and soil texture on species distribution within the environmental space. The resulting ordination axes were subsequently interpreted as synthetic gradients of moisture-related ecological variation and used to derive edaphic and topographic moisture-response scales.

The sampling support and structure of the resulting species–environment matrices across a broad range of environmental resolutions were evaluated to assess the sensitivity of the environmental discretization procedure to the number of bins [58]. Precipitation, TWI, and soil texture were independently discretized into 5, 10, 15, 20, or 25 bins, yielding 125 factorial combinations of bin numbers. For each combination, environmental cells were defined by the intersection of the three discretized predictors, and the resulting data structure was characterized by the number and proportion of occupied cells, the distribution of occurrence records among cells, the proportion of cells with low sampling support, species richness per cell, and species–environment matrix sparsity. These diagnostics were used to identify a range of environmental resolutions that retained adequate sampling and species representation without excessive matrix sparsity [59]. The subsequent CCA sensitivity analysis was then performed for all factorial combinations of 5, 10, and 15 bins for precipitation, TWI, and soil texture (27 discretization schemes). This two-stage procedure separated the computationally inexpensive assessment of environmental resolution and data support from the more computationally demanding evaluation of ordination stability. For the retained range of discretization resolutions, CCA was repeated for all 27 factorial combinations of 5, 10, and 15 bins for precipitation, TWI, and soil texture. Ordination stability was evaluated using the proportion of constrained inertia represented by the first three CCA axes, Procrustes correlation of species configurations relative to the $15 \times 15 \times 10$ solution, and consistency of the dominant environmental association of CCA1 and CCA2. The CCA was repeated using three alternative weighting schemes for the species-by-environmental-cell matrix to assess whether the constrained ordination structure was sensitive to differences in the representation of species occurrence frequencies [60]. The original analysis used raw numbers of occurrence records for each species within each environmental cell. This was compared with square-root-transformed abundances, which reduced the influence of highly represented species while retaining information on occurrence frequency, and with presence/absence data, in which each species contributed equally irrespective of the number of occurrence records within a cell [61,62]. Environmental discretization and the set of constraining predictors were kept unchanged among the

three analyses. Stability of the ordination was assessed by comparing the proportions of constrained inertia represented by CCA1–CCA3 and by Procrustes correlations of species configurations relative to the raw-abundance solution [57,63]. The consistency of ecological interpretation was additionally evaluated by identifying the environmental variable (precipitation, TWI, or soil texture) showing the strongest absolute Spearman correlation with the site scores of CCA1 and CCA2 under each weighting scheme. Because the orientation of ordination axes is arbitrary, environmental associations were compared by their absolute magnitude rather than by correlation sign.

The sensitivity of the CCA ordination to unequal environmental availability was assessed by estimating the spatial representation of each environmental supercluster across the European study domain [64,65]. Environmental availability was derived independently of species occurrence records from the 250 m raster layers of precipitation, TWI, and soil texture. The raster values were classified using the same environmental boundaries as those defining the 15 × 15 × 10 supercluster scheme in the occurrence dataset, and the proportional area occupied by each resulting environmental supercluster was calculated from the number of raster cells assigned to it. The original species-by-supercluster matrix was compared with two availability-corrected variants to evaluate whether differences in environmental availability affected the ordination. Species occurrences within each supercluster were weighted by the inverse square root of its proportional environmental availability in the first variant and by inverse proportional availability in the second. The former provided a moderate correction for unequal availability, whereas the latter represented full availability standardization. The environmental predictors and CCA specification were otherwise kept unchanged. Sensitivity was evaluated from changes in the proportions of constrained inertia represented by CCA1–CCA3, Procrustes correlations of species configurations relative to the uncorrected solution, and the environmental variable showing the strongest absolute Spearman correlation with CCA1 and CCA2 site scores [57,66]. Correlation magnitudes rather than signs were used to compare environmental associations because axis orientation is arbitrary in ordination. The sensitivity of the CCA ordination to variation in GBIF spatial sampling intensity was assessed using alternative levels of species-specific spatial thinning [67,68]. In addition to the 10 km thinning used in the primary analysis, occurrence data were independently thinned to retain a maximum of one record per species within 20 × 20 km and 30 × 30 km grid cells. For each thinning level, the environmental-supercluster procedure was repeated using the same 15 × 15 × 10 discretization of precipitation, TWI, and soil texture, respectively. Species-by-supercluster matrices were reconstructed from the retained occurrence records, and CCA was performed using the same environmental predictors and model specification. Sensitivity to spatial sampling intensity was evaluated by comparing the proportions of constrained inertia represented by CCA1–CCA3 and by calculating Procrustes correlations between species configurations obtained at the 20 and 30 km thinning levels and the 10 km reference solution. The consistency of the ordination interpretation was additionally assessed by identifying the environmental variable showing the strongest absolute Spearman correlation with CCA1 and CCA2 site scores at each thinning level. Correlation magnitudes rather than signs were compared because the orientation of ordination axes is arbitrary.

2.5. Spatial Extrapolation of Ordination Gradients

The CCA site scores were subsequently modelled explicitly as functions of annual precipitation, TWI, soil texture, and their interactions. For this purpose, annual precipitation was log-transformed, and all predictors were standardised. Separate linear models were fitted for the first and second CCA axes:

$$CCA_k = \beta_0 + \beta_1 P_{log} + \beta_2 TWI + \beta_3 Texture + \beta_4 P_{log} TWI + \beta_5 P_{log} Texture + \beta_6 TWI Texture + \beta_7 P_{log} TWI Texture,$$

where CCA_k is the score for CCA1 or CCA2.

The orientation of each CCA axis was established before rescaling on the basis of its ecological correspondence with the moisture gradients used for interpretation because the sign of an ordination axis is arbitrary. In particular, the fitted Didukh and Ellenberg moisture vectors were strongly aligned with the negative direction of CCA1; therefore, CCA1 was sign-reversed before transformation into EMI so that increasing EMI values represented progression from the dry to the wet end of the ecological moisture gradient. The subsequent linear transformation preserved this orientation while rescaling the index to the 1–23 range.

The models included the main effects of log-transformed annual precipitation (Plog), TWI, and soil texture coefficient (Texture), all three two-way interactions (Plog × TWI, Plog × Texture, and TWI × Texture), and the three-way interaction (Plog × TWI × Texture). The fitted regression coefficients were then applied to the raster stack of environmental predictors. For each 250 m grid cell, annual precipitation was log-transformed, and all predictors were standardised using the means and standard deviations obtained from the calibration dataset. Predicted CCA1 and CCA2 scores were calculated pixel-wise from the fitted models, resulting in two continuous raster layers representing the spatial expression of the ordination gradients across Europe. The predicted CCA1 and CCA2 raster layers were subsequently recalibrated to a 1–23 scale, corresponding to the numerical range of the Didukh ecological indicator system. Predicted ordination scores were linearly rescaled using the minimum and maximum values observed in the calibration dataset and constrained to the 1–23 interval. The resulting raster layers represent two synthetic moisture-related gradients derived exclusively from environmental variables. Their ecological interpretation as edaphically and topographically controlled components of moisture availability was subsequently established through calibration against independent phytoindication estimates.

2.6. Estimation and Calibration of Species-Level Moisture Indicator Values

The predicted edaphic and topographic moisture rasters were used to estimate species ecological niche positions along both synthetic gradients. For each species, raster values were extracted at all occurrence locations, and the 10th percentile, median, and 90th percentile were calculated to represent the lower limit, optimum, and upper limit of the species moisture niche, respectively. Species with insufficient numbers of occurrence records were excluded. These niche parameters were converted into species-level indicator values by rank-based rescaling to the numerical range of the Didukh moisture indicator system (1–23), preserving the relative ordering of species while ensuring direct comparability with the traditional scale. The topographic moisture gradient was retained in its calibrated form because no directly comparable phytoindication scale is currently available. In contrast, the edaphic moisture gradient showed strong but distinctly non-linear correspondence with the Didukh and Ellenberg moisture indicator systems. Therefore, the edaphic scale was recalibrated by rank-based distribution matching to produce a consensus scale integrating traditional phytoindication with occurrence-derived estimates. The relationships between occurrence-derived and traditional indicator values were evaluated using principal curve analysis. Lower niche limits were compared with Didukh minimum values, niche optima with Ellenberg moisture values (rescaled to the 1–23 range), and upper niche limits with Didukh maximum values. Principal curves fitted with smooth-spline smoothing were used to characterise the non-linear correspondence between the occurrence-derived edaphic

scale and the traditional phytoindication systems. Indicator values of the newly developed edaphic and topographic scales, together with the corresponding Ellenberg and Didukh values, are provided in the accompanying Zenodo dataset [69].

2.7. Community-Level Ecological Consistency of Moisture Indicator Scales

The ecological consistency of the traditional and newly derived moisture indicator scales was evaluated using a large dataset of vegetation plots. For each plot, species abundances were combined with their corresponding indicator values to calculate abundance-weighted mean moisture conditions and abundance-weighted within-community standard deviations. Within-community standard deviations were standardised by the total species-level standard deviation of the corresponding indicator system to enable comparison among scales with different numerical properties. The resulting relative within-community variation

$$relSD = \frac{SD_{\text{within community}}}{SD_{\text{all species}}}$$

was used as a measure of ecological coherence. Lower values indicate that species co-occurring within the same community possess more similar indicator values and therefore exhibit greater ecological consistency with respect to the evaluated gradient.

Relative variation was calculated separately for lower niche limits, niche optima, and upper niche limits. Differences between the traditional indicator system and the newly derived edaphic and topographic scales were evaluated using one-sided paired Wilcoxon signed-rank tests. The alternative hypothesis was that the traditional scales exhibit greater within-community variation than the newly derived scales. p-values were adjusted for multiple comparisons using the Benjamini–Hochberg procedure.

2.8. Explanatory Power of Moisture Indicator Scales

The explanatory power of both the traditional and newly derived moisture scales was assessed as an additional community-level evaluation using canonical correspondence analysis of vegetation plot data (Figure 3). The vegetation plot dataset used for this analysis comprises 10,931 relevés representing vascular plant community composition across the southeastern Ukrainian steppe zone. The dataset was compiled from regional vegetation surveys and was used to assess the spatial agreement between community-level moisture estimates and the derived moisture indicator scales. The complete species-by-relevé matrix and associated metadata are available in the public repository [70].

For each plot, abundance-weighted mean moisture values were calculated separately for the traditional Ellenberg moisture scale, the new edaphic moisture optimum, and the new topographic moisture optimum. These plot-level moisture indices were used as explanatory variables in separate CCA models, with the species composition matrix of vegetation plots used as the response matrix. The adjusted coefficient of determination was calculated for each model using RsquareAdj from the *vegan* package [71]. This allowed comparison of the amount of variation in species composition explained by each moisture scale. A combined model incorporating both edaphic and topographic moisture indices was fitted to determine whether the topographic scale provided additional explanatory power beyond the edaphic scale. Incremental explanatory power was assessed as the difference in adjusted R^2 between models.

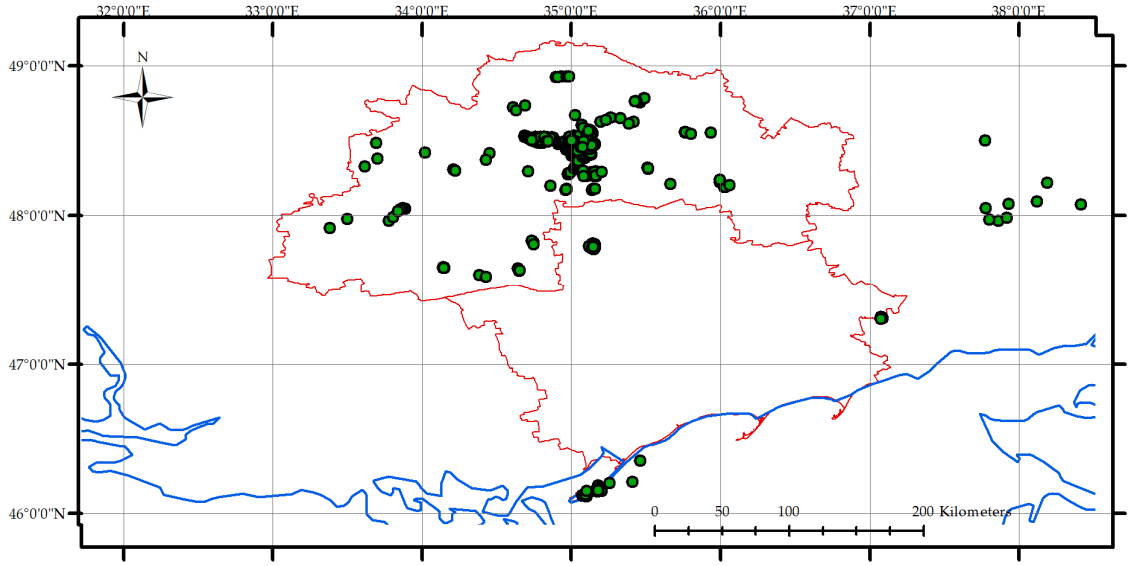


Figure 3. Spatial distribution of vegetation plots used for community-level assessment of the moisture indicator scales (n = 10,931). The red outline delineates the focal regions of the Ukrainian steppe zone, encompassing the Dnipropetrovsk and Zaporizhzhia regions. Additional plots from the steppe part of the Donetsk region were included to improve regional coverage of the assessment dataset.

2.9. Spatial Blocking and Validation of Community-Level Phytoindication Estimates

As a spatially blocked assessment of community-level phytoindication estimates, plot-level indicator values were compared with environmental moisture-gradient values extracted at the corresponding vegetation-plot locations. The coordinates of vegetation plots were converted to spatial points and projected to ETRS89/LAEA Europe (EPSG:3035), after which values of the edaphic moisture index (EMI) and topographic moisture index (TMI) raster layers were extracted for each plot. For each vegetation plot, abundance-weighted mean indicator values were calculated from the species composition matrix. Six community-level phytoindication estimates were considered: the traditional Didukh estimate, based on the mean of the lower and upper moisture limits; the traditional Ellenberg moisture estimate; the new edaphic estimates based on the mean of the lower and upper edaphic limits and on the edaphic optimum; and the corresponding topographic estimates based on the mean of the lower and upper topographic limits and on the topographic optimum. To account for the spatially clustered distribution of the 10,931 vegetation plots, validation was performed within spatial blocks rather than solely across the complete set of plot locations. The plots were initially aggregated into 2 × 2 km spatial microclusters in the projected coordinate system. This produced 193 microclusters, five of which contained single plots without valid EMI or TMI raster values and were excluded from the blocked assessment. Because many individual microclusters represented only a narrow portion of the regional moisture gradient, they were subsequently aggregated into larger validation blocks. Block construction simultaneously considered geographical proximity, sample size, and environmental-gradient coverage. Candidate neighbouring microclusters were progressively merged to increase coverage of the corresponding moisture gradient while limiting the increase in geographical separation. A validation block was considered sufficiently informative when it contained at least 100 vegetation plots and encompassed at least 30% of the regional robust environmental range, defined as the difference between the 95th and 5th percentiles of the corresponding raster-derived moisture gradient. Spatial blocks were constructed separately for EMI and TMI because the two indices represent distinct components of environmental moisture variation and differ in their regional ranges. The procedure produced 18 validation blocks for EMI and 14 validation blocks for TMI. All

resulting EMI blocks contained at least 108 vegetation plots and covered at least 30.4% of the regional 5–95th percentile EMI span; the corresponding values for TMI were at least 178 plots and 33.0% of the regional TMI span. Median block sizes were 352 plots for EMI and 405 plots for TMI, while median environmental coverage was 68.0% and 90.9% of the respective regional robust gradients. Within each validation block, the raster-derived moisture values were compared with each of the six community-level phytoindication estimates using Spearman's rank correlation. The distributions of block-specific Spearman coefficients were summarised by their median and interquartile range, and directional consistency was quantified as the number and proportion of validation blocks exhibiting positive correlations. Additionally, block-specific correlations were Fisher z-transformed, weighted by their effective sample size ($n - 3$), averaged, and back-transformed to obtain a pooled correlation coefficient. EMI and TMI were assessed separately using their respective spatial blocking structures. This procedure was employed to evaluate whether associations between community-level phytoindication estimates and the two environmental moisture components were reproducible across spatially differentiated subsets of the vegetation dataset, while retaining sufficient within-block environmental variation to estimate the relationships.

2.10. Landscape-Level Assessment of Consistency with Topographic and Remotely Sensed Moisture Indicators

Three representative landscape systems were analysed using georeferenced vegetation relevés to further evaluate the performance of the traditional and newly developed moisture indicator scales at the local landscape level: the psammophytic steppe landscape [23], the floodplain ecosystem complex of Khortytsia Island [72], and the ravine–valley landscape system of Mayorka Valley [44] (Figure 4). The vegetation relevés used in the landscape-level analyses were derived from original field surveys conducted by the authors. The corresponding primary species-occurrence records have been published as openly accessible datasets through the Global Biodiversity Information Facility (GBIF), ensuring transparency and reproducibility of the underlying biodiversity data [73]. Detailed descriptions of the sampling design, vegetation plot methodology, species recording procedures, and original datasets are provided in the corresponding publications and openly available data repositories.

For each system, a species-by-plot matrix was compiled from field vegetation descriptions, with species cover values used as weights. Plot-level phytoindication estimates were calculated as abundance-weighted means of species indicator values. The following moisture estimates were calculated for each plot: the traditional Didukh estimate, obtained as the mean of the lower and upper Didukh moisture limits; the traditional Ellenberg moisture estimate; the new edaphic moisture estimate based on the mean of the lower and upper edaphic limits; the new edaphic optimum; the new topographic moisture estimate based on the mean of the lower and upper topographic limits; and the new topographic optimum. Local terrain controls on moisture redistribution were characterised using a digital elevation model. The DEM was hydrologically corrected by filling depressions, after which slope and specific contributing area were calculated using WhiteboxTools [74]. The Topographic Wetness Index was then computed as

$$TWI = \ln\left(\frac{SCA}{\tan(\beta)}\right),$$

where SCA is the specific contributing area and β is the local slope angle in radians. A minimum slope threshold of 0.5° was applied to avoid instability in nearly flat areas. TWI values were extracted for all vegetation plot locations.

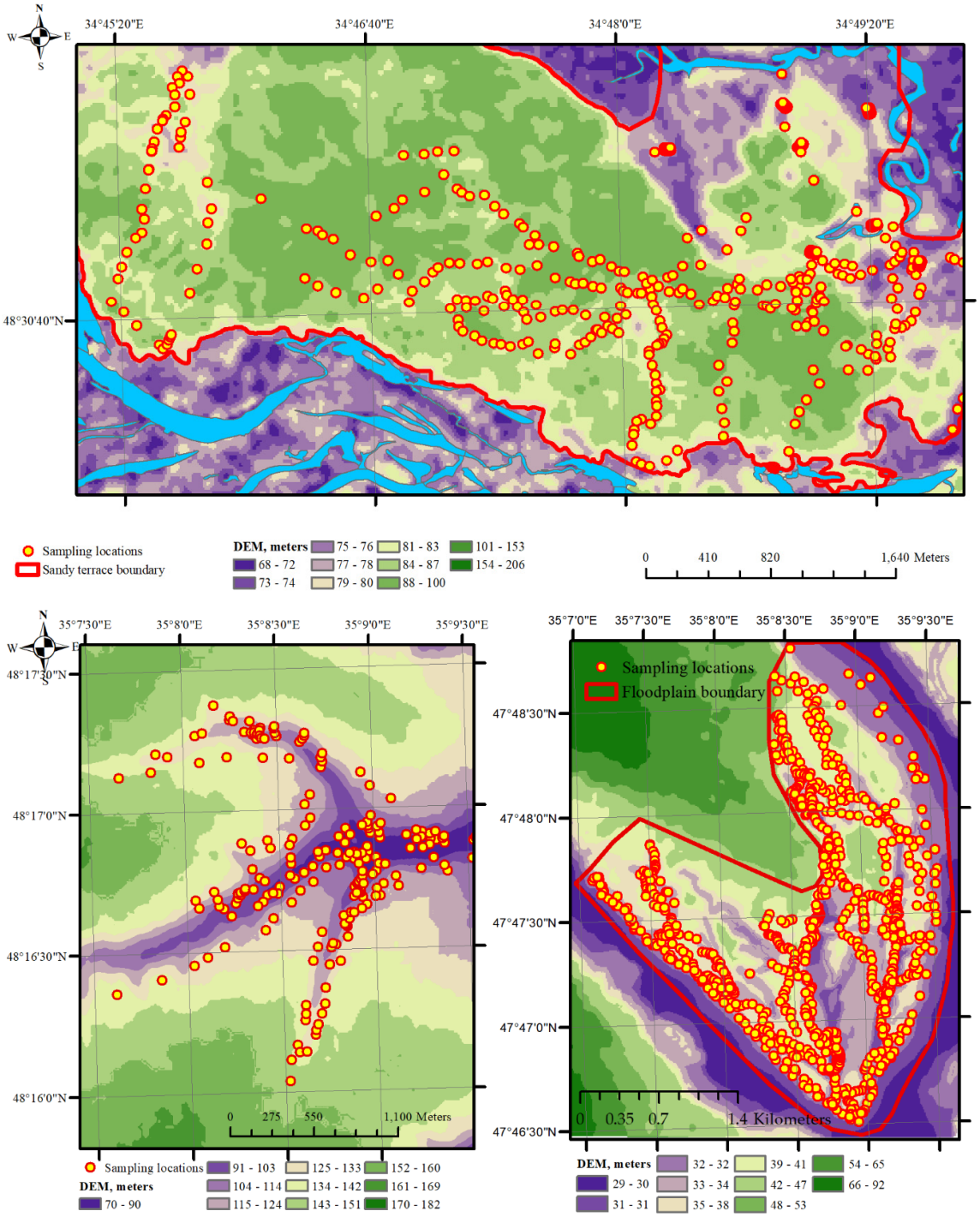


Figure 4. Spatial distribution of vegetation plots within the three landscape systems used for local-scale assessment of moisture indicator scales. Upper panel: psammophytic steppe landscape. Lower left panel: Mayorka Valley ravine–valley landscape system. Lower right panel: floodplain ecosystem complex of Khortytsia Island. Orange circles indicate vegetation plot locations. Red polygons delineate the boundaries of the analysed landscape systems. Background colours represent elevation derived from digital elevation models (DEMs). The three landscapes encompass contrasting geomorphological and hydrological settings and were used to evaluate the performance of traditional and newly developed moisture indicator scales under local environmental conditions.

At the landscape level, NDWI was used as an independent remote-sensing proxy of local moisture conditions [75]. NDWI was calculated from Sentinel imagery acquired close to the dates of vegetation sampling, which was conducted from late July to early August in

all three landscape systems. Sentinel-2 imagery was processed according to the procedures described in [76,77]. The index was calculated as

$$NDWI = \frac{NIR - SWIR}{NIR + SWIR},$$

where NIR and SWIR are the near-infrared and short-wave infrared spectral bands, respectively, higher NDWI values indicate greater surface or vegetation-related moisture availability. Sentinel-2 MSI Level-2A surface reflectance products were used, with the B8 near-infrared and B11 short-wave infrared bands employed for NDWI calculation. Cloud- and cloud-shadow-affected pixels were excluded using the Sentinel-2 quality layers, and the spectral bands were geometrically aligned to a common raster grid. The final NDWI raster layers were produced at a spatial resolution of 10 m, with the 20 m SWIR band resampled to the 10 m reference grid. For comparison with field observations, cloud-free Sentinel-2 acquisitions were selected to minimise the temporal difference between satellite acquisition and field sampling; when an image from the exact sampling date was unavailable, the nearest suitable acquisition was used.

Field measurements of soil moisture were conducted on Khortytsia Island (Ukraine) during late July and August of 2024 and 2025. Soil moisture was measured at 878 vegetation plot locations using an MG–44 soil moisture meter (Ukraine). Measurements were taken at a soil depth of 5–7 cm. The device provides a measurement resolution of 0.1% with an estimated measurement error of 1%. The field measurements were used to evaluate the relationship between directly measured soil moisture and the satellite-derived Normalized Difference Water Index (NDWI). NDWI values were extracted from Sentinel imagery acquired as close as possible to the dates of field measurements, including images from 14 July, 18 August, and 23 August 2024, and from 14 July, 19 July, 29 July, 8 August, 13 August, 18 August, and 28 August 2025. Field moisture measurements showed a statistically significant positive relationship with NDWI. The regression model indicated that NDWI explained approximately 11.7% of the variation in measured moisture conditions ($R^2 = 0.117$, adjusted $R^2 = 0.116$, $F = 116.41$, $p < 0.001$). The regression coefficient for NDWI was positive ($\beta = 0.342$, $p < 0.001$), confirming that higher NDWI values corresponded to higher field-measured moisture. Therefore, NDWI was used as an independent remote-sensing proxy of local moisture availability for landscape-level assessment of the indicator scales.

The NDWI-derived moisture proxy was regressed against DEM-derived TWI to separate the topographically structured component of local moisture from residual variation. The fitted values of this model were interpreted as the TWI-predicted component of moisture, whereas residuals represented moisture variation not explained by local topographic wetness. Both variables were then added to the plot-level dataset and compared with community-level phytoindication estimates derived from the traditional Didukh and Ellenberg scales, the new edaphic scale, and the new topographic scale. This allowed assessment of whether different indicator systems were more closely associated with the topographically predictable or residual component of local moisture variation.

2.11. Null-Model Analysis of Community Moisture Indicator Values

Standardised effect sizes (SESs) [78] were calculated for each indicator scale to assess whether community-level phytoindication estimates showed non-random structure along local moisture gradients. For each vegetation plot, the observed abundance-weighted mean indicator value was compared with a null distribution generated by random permutation of species indicator values. Species cover values and the species composition of each plot were kept unchanged, whereas indicator values were randomly reassigned among species.

This procedure was repeated 999 times for each scale. The standardised effect size was calculated as

$$SES = \frac{I_{obs} - \mu_{null}}{\sigma_{null}},$$

where I_{obs} is the observed abundance-weighted mean indicator value, μ_{null} is the mean of the null distribution obtained by random permutation of species indicator values, and σ_{null} is the corresponding standard deviation. Values of SES greater than 1.645 or lower than -1.645 were interpreted as indicating significant positive or negative deviation from random expectation at the one-sided 5% level.

SES values were then related to two components of the NDWI-derived moisture proxy: the TWI-predicted component and the residual component not explained by TWI. This allowed evaluation of whether traditional and newly developed indicator scales captured topographically structured moisture variation or residual local moisture variability. SES values were divided into three zones for more detailed interpretation of standardised effect sizes: neutral, positive deviation from the random expectation, and negative deviation from the random expectation. Neutral values were defined as ($|SES| \leq 1.645$), indicating no significant deviation from the null expectation. Positive deviations (SES > 1.645) indicate that community-weighted mean indicator values were significantly higher than expected under the null model, whereas negative deviations (SES < -1.645) indicate significantly lower values than expected by chance. The proportion of plots with significantly positive, significantly negative, or non-significant SES values was calculated for each indicator scale. The relationship between SES and local moisture gradients was analysed separately for the positive and negative SES groups. Both the moisture variable and SES were standardised before modelling, and linear slopes were estimated for each zone. Statistical significance of positive slopes was assessed by permutation tests in which SES values were randomly permuted 999 times within each zone. This analysis allowed assessment of whether non-random phytoindication signals were systematically structured along the TWI-predicted and residual components of NDWI-derived moisture variability.

Spatial dependence in the three local landscape datasets (Khortytsia, Mayorka, and Psammophytic steppe) was explicitly accounted for using spatially blocked validation. The characteristic scale of spatial autocorrelation was first estimated separately for each landscape from empirical variograms of measured soil moisture and the topographic wetness index (TWI). Spherical, exponential, and Gaussian variogram models were fitted to the empirical variograms, and the model with the lowest residual sum of squares was retained. Effective autocorrelation ranges were calculated according to the fitted model. For measured soil moisture, the estimated effective ranges were 568 m for Khortytsia, 243 m for Mayorka, and 140 m for the Psammophytic steppe. These distances were subsequently used as landscape-specific thresholds for defining spatial dependence units. Within each landscape, sampling plots were grouped into spatial dependence units by hierarchical clustering of their Euclidean spatial distances using complete linkage, with the dendrogram cut at the corresponding effective autocorrelation range. The resulting units, rather than individual plots, were then assigned to five spatial validation folds based on the spatial positions of their centroids, ensuring that plots belonging to the same spatial dependence unit were retained within the same fold. The robustness of the relationships between measured soil moisture and phytoindication estimates was evaluated across these five spatial folds. Spearman rank correlations were calculated separately within each fold and summarized across folds by the median and interquartile range. The same spatial partitioning was applied to the standardized effect size (SES) diagnostics. For each phytoindication scale, the proportions of plots falling within the random expectation (| SES | \leq 1.645), above the random expectation (SES > 1.645), and below the random expectation (SES < -1.645) were calculated separately for each spatial

fold and subsequently summarized as medians and interquartile ranges across the five folds. This spatially blocked procedure was used to determine whether the observed phytoindication patterns were consistently reproduced across spatially separated subsets of each landscape rather than being driven by local spatial dependence among neighbouring vegetation plots.

2.12. Assessment of Ecological Consistency with the Belgard–Tarasov Hygromorph Classification

As an additional assessment, the traditional and newly developed moisture indicator scales were compared with the Belgard–Tarasov hygromorph classification [48]. This system represents an expert-based ecological classification of plant species according to their moisture preferences and is widely used in Eastern European phytocoenology. Hygromorph categories were treated as an ordinal gradient ranging from extreme xerophytes to aquatic plants. For quantitative comparison, hygromorph classes were converted into an ordered numerical sequence: EuXero (1), Xero (2), MsXero (3), XeroMs (4), Ms (5), HgMs (6), MsHg (7), Hg (8), Pl (9), and Hy (10). Species-level values of the traditional Didukh and Ellenberg moisture scales, the newly developed edaphic moisture scales, and the newly developed topographic moisture scales were then compared with the corresponding hygromorph scores. Relationships between hygromorph categories and moisture indicator values were visualised using scatterplots with fitted linear regression lines and 95% confidence intervals. Because hygromorph classes represent an ordinal rather than an interval scale, the strength of association was quantified using Spearman's rank correlation coefficient. This analysis provided an assessment of the agreement between the moisture scales and an alternative expert-based classification system that was not used during scale development.

3. Results

3.1. Sensitivity to Environmental Discretization, Record Weighting, Environmental Availability, and GBIF Sampling Intensity

A total of 125 environmental discretization schemes were evaluated, representing all combinations of 5, 10, 15, 20, and 25 bins for precipitation, TWI, and soil texture. Table S1 summarizes the symmetric combinations, which most clearly illustrate the general effect of increasing environmental resolution on sampling support and species–environment matrix structure. Resolutions of 5–15 bins retained strong sampling support: all environmental cells were occupied, median cell richness remained high (816–1437 species), and the proportion of cells represented by fewer than 100 records did not exceed 0.30%. At finer resolutions, sampling support declined more markedly, with the proportion of poorly represented cells increasing to 1.70% at 20 bins and 5.09% at 25 bins, accompanied by substantially greater matrix sparsity. Based on these diagnostics, subsequent CCA sensitivity analyses were restricted to all combinations of 5, 10, and 15 bins for each environmental factor, representing a broad range of well-supported discretization alternatives without extending into resolutions increasingly affected by sparse cell representation. Sensitivity analysis across 27 factorial combinations of environmental discretization (5, 10, and 15 bins for precipitation, TWI, and soil texture) showed very high stability of the constrained ordination structure (Table S2). Procrustes correlations between species configurations and the reference ordination ranged from 0.990 to 1.000 (median = 0.997). The proportion of constrained inertia represented by CCA1 varied only from 32.3% to 33.6%, whereas CCA2 accounted for 23.7–24.3%. Importantly, the environmental interpretation of the axes was invariant across all tested discretization schemes: soil texture was the dominant correlate of CCA1 in all 27 models, while TWI was the dominant correlate of CCA2 in all 27 models. These results indicate that the principal constrained compositional structure was consistently reproduced across alternative discretization schemes using 5, 10, and

15 bins for each environmental factor, demonstrating that the ordination structure was not dependent on a particular choice of environmental discretization.

The constrained ordination was also robust to alternative treatments of occurrence frequency (Table S3). Species configurations obtained using square-root-transformed abundance and presence/absence data remained strongly congruent with the raw-abundance solution (Procrustes r = 0.971 and 0.921, respectively). Weighting affected the relative contribution of the constrained axes, with the proportion of constrained inertia represented by CCA1 increasing from 32.8% for raw abundance to 43.2% for square-root-transformed abundance and 50.1% for presence/absence data, whereas CCA2 remained comparatively stable (22.2–24.0%). Importantly, the dominant environmental associations of the first two axes were retained under all three weighting schemes: CCA1 was most strongly associated with soil texture, whereas CCA2 was most strongly associated with TWI. Thus, the principal ecological structure of the ordination was not dependent on the use of raw occurrence frequencies in the species–environment matrix.

The sensitivity of the CCA solution to unequal environmental availability was assessed by comparing the original ordination with two alternative treatments in which species occurrences within environmental superclusters were weighted by inverse square-root availability and inverse availability, respectively (Table S4). Environmental availability was estimated from the spatial extent of each environmental supercluster across Europe using the environmental raster layers. Availability varied substantially among superclusters, with the area of the most widespread combination exceeding the median supercluster area by approximately 31-fold. Despite this variation, the principal ordination structure was retained after availability correction. Procrustes congruence with the uncorrected solution was 0.922 under inverse square-root availability weighting and 0.805 under full inverse-availability weighting. CCA1 consistently accounted for 31.4–33.5% of constrained inertia and was most strongly associated with soil texture (ρ = 0.769–0.790), whereas CCA2 accounted for 24.0–27.8% and was most strongly associated with TWI ($|\rho|$ = 0.715–0.796). Thus, correction for unequal environmental availability affected the detailed species configuration but did not change the dominant environmental associations of the first two constrained axes.

The sensitivity of the CCA ordination to variation in GBIF spatial sampling intensity was assessed by progressively increasing species-specific spatial thinning from 10 to 20 and 30 km (Table S5). This reduced the number of retained occurrence records from 4.55 million at 10 km to 2.78 million at 20 km and 1.97 million at 30 km. Despite this substantial reduction in occurrence records, the species configurations remained highly congruent with the 10 km solution, with Procrustes correlations of 0.996 and 0.990 for the 20- and 30 km solutions, respectively. The relative contribution of the first three constrained axes also remained similar: CCA1 accounted for 39.7–44.6% of constrained inertia, CCA2 for 23.2–23.8%, and CCA3 for 15.0–17.5%. Importantly, the dominant environmental associations of the first two axes were retained across all thinning levels. CCA1 remained most strongly associated with soil texture (ρ = 0.742–0.772), whereas CCA2 remained most strongly associated with TWI ($|\rho|$ = 0.612–0.734). Thus, the principal ordination structure and the dominant environmental associations of CCA1 and CCA2 were highly stable under substantially increased spatial thinning of the GBIF occurrence data.

3.2. Complementary Edaphic Storage and Climatic–Topographic Redistribution Dimensions of the Moisture Regime

The constrained CCA ordination revealed a multidimensional structure of species compositional turnover within the environmental space defined by precipitation, topographic wetness index (TWI), and soil texture. The first constrained axis (CCA1), accounting for 32.8% of the constrained inertia, was most strongly associated with the texture coefficient,

while the fitted phytoindication vectors of moisture (Didukh minimum, Didukh maximum, and Ellenberg F values) were aligned with the negative direction of this axis (Table 1). This pattern supports the interpretation of CCA1 as a constrained compositional gradient predominantly associated with the edaphic component of moisture availability, particularly variation in soil water-retention conditions. The second constrained axis (CCA2), accounting for an additional 23.9% of the constrained inertia, was associated with contrasting contributions of precipitation and TWI. This pattern is consistent with a compositional response component associated with climatic moisture supply and topographically mediated redistribution, accumulation, and drainage of water. All fitted phytoindication moisture vectors were significant ($p = 0.001$) and showed strong associations with the constrained ordination structure ($R^2 = 0.76$–0.80). These values quantify the correspondence of the conventional phytoindication vectors with the ordination configuration and are not interpreted as independent validation of the environmental model. The contrasting associations of CCA1 and CCA2 with the physical predictors indicate that compositional variation related to moisture conditions cannot be adequately represented by a single constrained gradient. Within the environmental space considered here, the first two constrained axes therefore distinguish two complementary response components: one predominantly associated with edaphic water-retention conditions and another associated with climatic supply and topographically mediated moisture redistribution.

Table 1. Constrained predictors and fitted moisture vectors in the CCA space.

	Predictor	CCA1	CCA2
Constrained	Precipitation (P)	−0.28	0.71
	Topographic wetness index (TWI)	−0.41	−0.87
	Texture coefficient (TC)	0.80	−0.01
	P × TWI	−0.60	−0.10
	P × TC	0.42	0.45
	TWI × TC	0.50	−0.47
	P × TWI × TC	0.25	−0.05
Fitted	Didukh_min ($R^2 = 0.76$)	−0.97	−0.24
	Didukh_max ($R^2 = 0.79$)	−0.99	−0.17
	Ellenberg_F ($R^2 = 0.80$)	−0.98	−0.21

The Didukh and Ellenberg moisture indicator scales showed similar associations with the environmental variables (Figure 5). TWI accounted for the largest proportion of variation in these conventional indicator values ($R^2 = 0.30$–0.35), followed by precipitation ($R^2 = 0.18$–0.22) and soil texture ($R^2 = 0.13$–0.14). The constrained compositional axes showed a different pattern of association: CCA1 was most strongly related to soil texture ($R^2 = 0.48$), whereas CCA2 was most strongly related to TWI ($R^2 = 0.61$). These relationships are used here to characterize the environmental interpretation of the constrained axes rather than as independent measures of ecological explanatory power. The contrast suggests that conventional phytoindication values primarily represent an integrated moisture gradient, whereas the constrained species-composition structure differentiates edaphic and topographically associated components within that gradient. The regression analysis further characterized the response surfaces of the conventional Ellenberg moisture indicator and the two CCA-derived compositional gradients in the environmental predictor space (Table 2). For Ellenberg values, positive coefficients for precipitation and TWI indicate increasing indicator values under wetter climatic and topographic conditions, whereas the negative coefficient for soil texture reflects variation associated with substrate water-retention properties. Significant precipitation × TWI and precipitation × texture interactions indicate that the fitted Ellenberg response surface varies jointly with climatic

moisture supply, local relief, and substrate properties. The three-way interaction was not significant, indicating that this response surface was adequately characterized primarily by the main effects and pairwise interactions considered in the model.

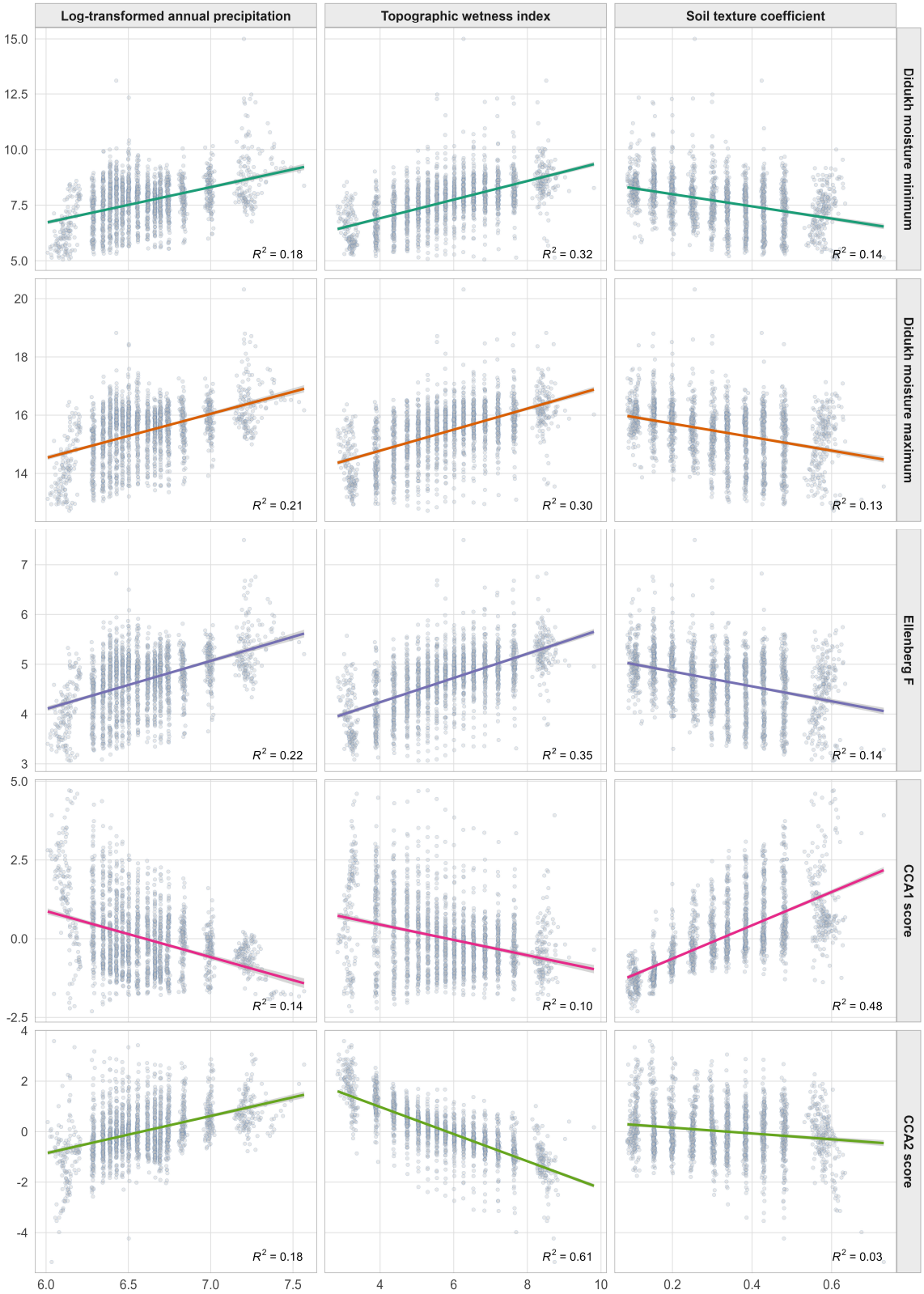


Figure 5. Relationships of ecological moisture indicator values and CCA ordination scores with climatic, topographic and edaphic predictors. Scatterplots show the relationships between phytoindication moisture

scales (Didukh minimum, Didukh maximum and Ellenberg F values), as well as CCA1 and CCA2 vegetation-composition scores, and three environmental predictors: log-transformed annual precipitation, topographic wetness index (TWI) and soil texture coefficient. Blue lines indicate linear regression fits, and panels display coefficients of determination (R^2). The results demonstrate that phytoindication moisture values are positively associated with precipitation and TWI, and negatively associated with soil texture. In contrast, CCA1 scores are strongly related to soil texture, whereas CCA2 scores primarily reflect variation associated with TWI.

Table 2. Linear regression models describing the responses of the CCA vegetation-composition axes to precipitation, TWI and soil texture. Predictors were centred and standardised before model fitting.

Response	Predictor	Estimate	Std. Error	*t*-Value	*p*-Value
Ellenberg indicator value. Model summary: residual standard error = 0.290; R^2 = 0.746; adjusted R^2 = 0.746; $F_{7,2242}$ = 942.6; $p < 0.001$.	Intercept	4.672	0.006	763.42	<0.001
	$P_{log,c}$	0.267	0.006	43.65	<0.001
	TWI_c	0.343	0.006	56.15	<0.001
	$Texture_c$	−0.218	0.006	−35.52	<0.001
	$P_{log,c} \times TWI_c$	−0.033	0.006	−5.46	<0.001
	$P_{log,c} \times Texture_c$	0.060	0.006	10.08	<0.001
	$TWI_c \times Texture_c$	0.094	0.006	15.28	<0.001
	$P_{log,c} \times TWI_c \times Texture_c$	−0.002	0.006	−0.26	0.799
CCA1. Model summary: residual standard error = 0.482; R^2 = 0.808; adjusted $R^2 = 0.808$; $F_{7,2242} = 1344.9$, $p < 0.001$.	Intercept	0.012	0.010	1.22	0.249
	$P_{log,c}$	−0.402	0.010	−39.43	<0.001
	TWI_c	−0.350	0.010	−34.40	<0.001
	$Texture_c$	0.767	0.010	75.37	<0.001
	$P_{log,c} \times TWI_c$	0.064	0.010	6.36	<0.001
	$P_{log,c} \times Texture_c$	−0.222	0.010	−22.47	<0.001
	$TWI_c \times Texture_c$	−0.257	0.010	−25.22	<0.001
	$P_{log,c} \times TWI_c \times Texture_c$	0.068	0.010	7.03	<0.001
CCA2. Model summary: residual standard error = 0.349; R^2 = 0.868; adjusted R^2 = 0.868; $F_{7,2242} = 2106.3$; $p < 0.001$.	Intercept	0.022	0.007	2.99	<0.001
	$P_{log,c}$	0.410	0.007	55.52	<0.001
	TWI_c	−0.743	0.007	−100.91	<0.001
	$Texture_c$	−0.152	0.007	−20.64	<0.001
	$P_{log,c} \times TWI_c$	0.060	0.007	8.27	<0.001
	$P_{log,c} \times Texture_c$	0.206	0.007	28.74	<0.001
	$TWI_c \times Texture_c$	0.084	0.007	11.34	<0.001
	$P_{log,c} \times TWI_c \times Texture_c$	−0.023	0.007	−3.35	<0.001

The fitted response surface for CCA1 had a structure broadly similar to that of the Ellenberg moisture gradient, although the arbitrary sign orientation of the CCA axis was reversed. The response-surface model reproduced CCA1 scores closely (R^2 = 0.81), with soil texture providing the dominant contribution and with substantial interaction terms. Because CCA1 was itself derived from an ordination constrained by the same environmental variables, this R^2 represents the goodness of reconstruction of the CCA-derived gradient in environmental predictor space and is not an independent estimate of ecological explanatory power. The model was used to parameterize the functional relationship between the CCA-derived compositional gradient and measurable environmental predictors for subsequent spatial prediction. The corresponding response-surface model reproduced CCA2 scores with R^2 = 0.87. Again, this value describes reconstruction of the constrained compositional gradient rather than independent explanatory performance. The fitted CCA2 response surface was dominated by TWI, supporting its interpretation as a compositional response component associated primarily with topographically mediated moisture redistribution. Thus, the two CCA axes provide distinct constrained representations of species-compositional responses within the same environmental predictor space: CCA1 emphasizes the texture-associated edaphic component, whereas CCA2 emphasizes the topographically associated redistribution component. Their distinction is based on their

contrasting environmental associations and fitted response structures, rather than on the mathematical orthogonality of the ordination axes alone.

3.3. Explicit Formulation of Edaphic and Topographic Moisture Gradients

The calibrated ordination models were subsequently transformed into two continuous moisture gradients scaled to the numerical range of the Didukh moisture indicator system (1–23). The resulting indices can be expressed as

$$\begin{aligned} EMI &= 15.73 + 1.26P_c + 1.10TWI_c - 2.41Texture_c - 0.20P_cTWI_c + 0.70P_cTexture_c + 0.81TWI_cTexture_c \\ &\quad - 0.21P_cTWI_cTexture_c \\ TMI &= 14.04 + 1.03P_c - 1.87TWI_c - 0.38Texture_c + 0.15P_cTWI_c + 0.52P_cTexture_c + 0.21TWI_cTexture_c \\ &\quad - 0.06P_cTWI_cTexture_c \end{aligned}$$

where EMI is the Edaphic Moisture Index and TMI is the Topographic Moisture Index.

$$P_c = \frac{\ln(P) - 6.59}{0.28}, TWI_c = \frac{TWI - 5.79}{1.39}, Texture_c = \frac{Texture - 0.32}{0.14}$$

Here, P denotes annual precipitation (mm), TWI is the Topographic Wetness Index, and $Texture$ is the soil-texture coefficient derived from the sand-to-clay ratio. Both indices were constrained to the interval 1–23, making them directly comparable with the traditional Didukh moisture indicator scale.

The two indices represent complementary dimensions of moisture availability. The Edaphic Moisture Index primarily reflects variations associated with soil-mediated water retention and climatic water supply, whereas the Topographic Moisture Index captures variations associated with topographically driven redistribution and accumulation of water within landscapes.

The calibrated environmental models made it possible to integrate precipitation, TWI, and soil texture into two synthetic moisture gradients representing complementary dimensions of moisture availability. The application of the fitted models to the environmental raster layers produced continuous maps of edaphic and topographic moisture conditions across southeastern Ukraine (Figure 6).

The edaphic moisture gradient exhibited pronounced spatial heterogeneity associated with broad-scale variation in climatic water supply and soil water-retention properties. Higher values were concentrated in areas characterized by greater precipitation and finer-textured soils, whereas lower values predominated in drier regions and areas with coarser soil texture. In contrast, the topographic moisture gradient emphasized local patterns of water redistribution controlled by terrain configuration. Elevated values occurred primarily in valleys, floodplains, and other topographically convergent positions where water accumulation is favoured, while lower values were associated with elevated and well-drained landscape positions. Together, these results demonstrate that the environmental predictors were successfully integrated into two interpretable moisture gradients that capture different components of landscape moisture variability. The edaphic gradient primarily reflects regional-scale variation in moisture availability related to climate and soil properties, whereas the topographic gradient represents local-scale variation associated with terrain-driven redistribution of water.

Principal curve analysis revealed a pronounced non-linear relationship between the occurrence-derived edaphic moisture estimates and the traditional moisture indicators of Didukh and Ellenberg (Figure 7).

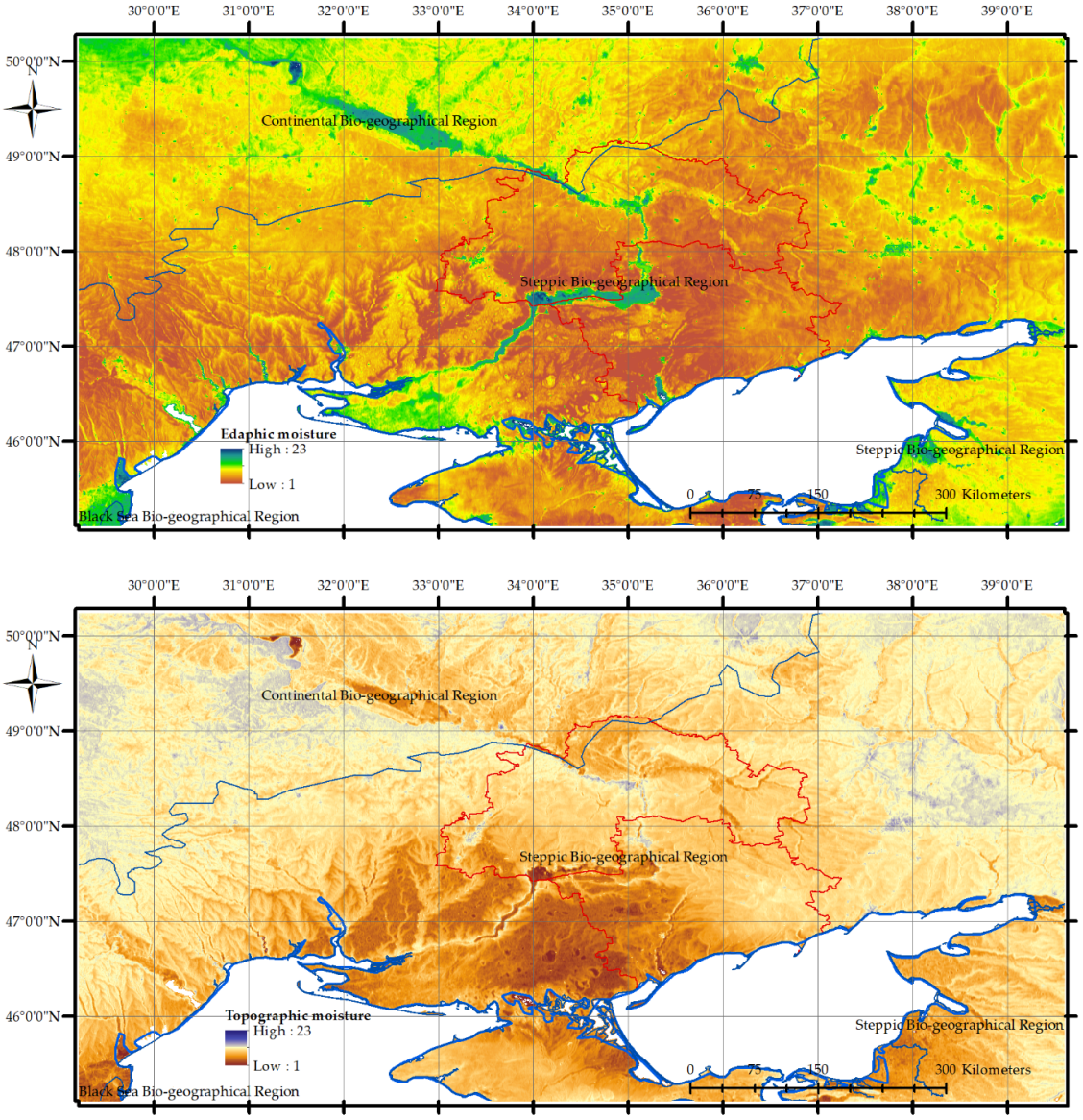


Figure 6. Spatial distribution of the rescaled edaphic and topographic moisture gradients across southeastern Ukraine. The upper panel shows the edaphic moisture gradient, whereas the lower panel shows the topographic moisture gradient. Both gradients were derived from environmental predictors through canonical correspondence analysis and subsequent regression modelling and were recalibrated to the 1–23 numerical range of the Didukh ecological indicator system. Higher values indicate wetter environmental conditions, while lower values correspond to drier conditions. Red outlines delineate the focal study regions used for calibration and assessment of the indicator scales. Boundaries of the Black Sea, Continental, and Steppe biogeographical regions are shown for geographic reference.

The strongest departures from linearity occurred in the intermediate part of the gradient, whereas the relationships approached saturation at both dry and wet extremes. In contrast, the topographic moisture scale showed no clear correspondence with the traditional indicator systems, suggesting that it represents a distinct dimension of moisture variability associated with topographically mediated redistribution of water, rather than with the edaphic moisture conditions reflected by conventional phytoindication scales.

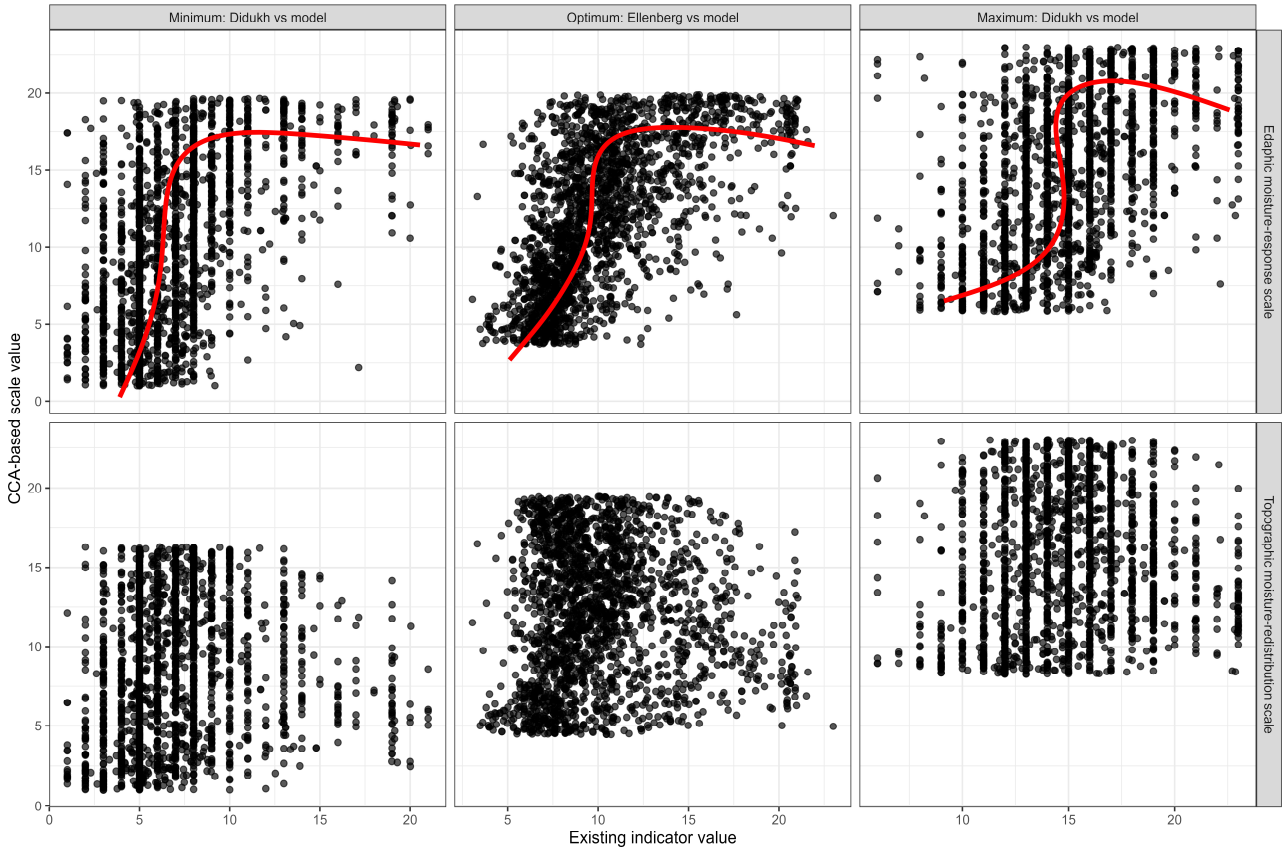


Figure 7. Relationships between traditional moisture indicator values and the CCA-derived moisture gradients. The upper panels show comparisons between the edaphic moisture scale and the corresponding traditional indicators (Didukh minimum moisture, Ellenberg moisture optimum, and Didukh maximum moisture), whereas the lower panels show analogous comparisons for the topographic moisture scale. Red curves represent principal curves fitted to visualize the dominant non-linear trend in the data. The edaphic moisture scale exhibits a strong but distinctly non-linear correspondence with the traditional indicator systems, while the topographic moisture scale shows little association with existing phytoindication values, indicating that it captures a complementary component of moisture variability not represented by conventional moisture indicators.

3.4. Within-Community Variation in Moisture Indicator Values Across Alternative Moisture Scales

As an indirect measure of the ecological consistency of moisture indicator values, the relative within-community variation in species moisture estimates was quantified for each scale. A reduction in within-community variation is expected if species scores more accurately reflect the moisture conditions shared by species co-occurring within the same plant community. The substantial within-location variation in species moisture indicator values across all three moisture parameters (minimum, optimum, and maximum), with median relative weighted standard deviations generally ranging from 0.34 to 0.55, was recorded (Figure 8).

The magnitude of this variation differed systematically among the traditional, edaphic, and topographic scales. The new edaphic scale exhibited lower within-location variation than the traditional scale (median relative SD = 0.383 vs. 0.451; median difference = 0.069) for the minimum moisture estimate, whereas the topographic scale showed slightly higher variation (0.467 vs. 0.451; median difference = −0.024). Both differences were statistically significant according to paired Wilcoxon tests (adjusted $p < 0.001$). The traditional scale produced the lowest variation among the three approaches for the optimum moisture estimate. Relative variation increased in the edaphic scale (median relative SD = 0.380 vs. 0.344; median difference = −0.025) and increased even more strongly in the topographic scale

(0.515 vs. 0.344; median difference = −0.143). Both contrasts were highly significant (adjusted $p < 0.001$). The edaphic scale again reduced within-location variation relative to the traditional scale (median relative SD = 0.440 vs. 0.513; median difference = 0.042; adjusted $p < 0.001$) for the maximum moisture estimate. In contrast, the topographic scale produced slightly greater variation than the traditional scale (0.544 vs. 0.513; median difference = −0.058; adjusted $p < 0.001$).

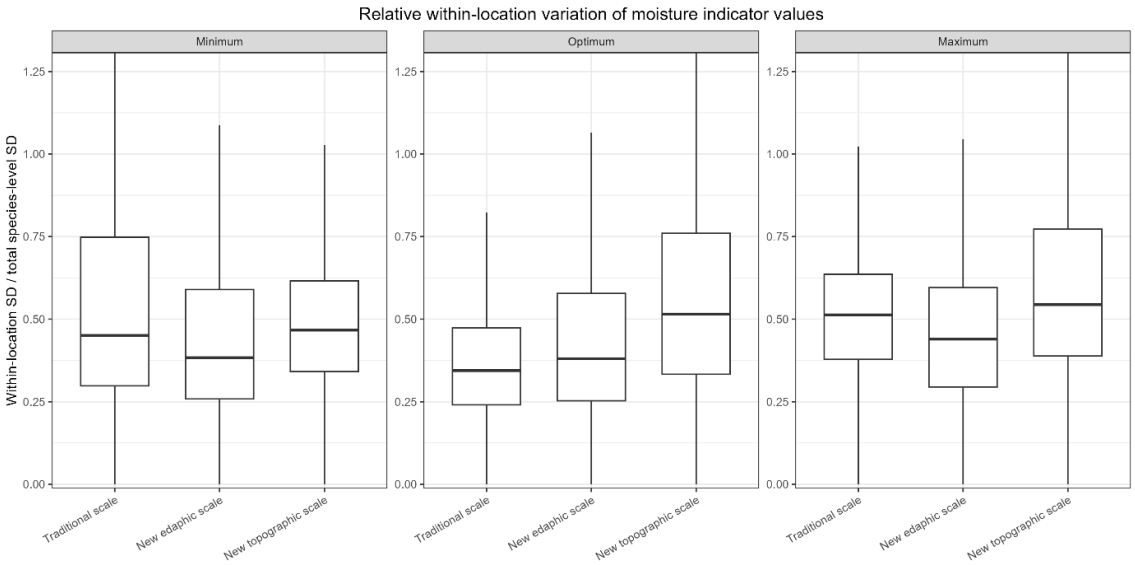


Figure 8. Relative within-location variability of moisture indicator values for the traditional, edaphic and topographic moisture scales. Variability was calculated as the ratio of the within-location weighted standard deviation to the total species-level standard deviation of the corresponding scale. Boxplots show the distribution of relative variability across 10,931 vegetation plots for minimum, optimum, and maximum moisture indicator values. Lower values indicate greater within-community consistency of indicator values.

The revised edaphic moisture scale reduced within-location heterogeneity for the minimum and maximum moisture components, indicating improved ecological consistency of species scores at these ends of the moisture gradient. In contrast, the topographic moisture scale generally increased within-location variation, particularly for optimum moisture, suggesting that topographic moisture estimates capture additional environmental differentiation among species occurring within the same locations. All pairwise comparisons were statistically significant after Benjamini–Hochberg correction (adjusted $p < 0.001$). Despite highly significant differences among scales, the observed patterns were parameter dependent, with the revised scales reducing within-community variation for some moisture characteristics and increasing it for others. Therefore, the results indicate scale-specific differences rather than a clear overall advantage of the revised approaches over the traditional moisture scale.

3.5. Explanatory Power of Moisture Scales for Community Composition

Single-factor CCA models revealed a similar strength of association between species composition and the traditional and edaphic moisture scales. The traditional moisture scale yielded the highest adjusted coefficient of determination (Adjusted R^2 = 0.0127; F = 140.0; p = 0.001), whereas the edaphic moisture component showed a nearly identical value (Adjusted R^2 = 0.0124; F = 136.0; p = 0.001). The topographic moisture component accounted for a smaller proportion of variation in species composition (Adjusted R^2 = 0.0074; F = 81.9; p = 0.001). When the edaphic and topographic moisture components were included in the same CCA model, the explained variation increased compared with the

single-component models (Adjusted R^2 = 0.0197). The combined model therefore explained more variation than the edaphic component alone (ΔAdjusted R^2 = 0.0073). In contrast, the edaphic component alone showed a nearly identical explanatory power to the traditional moisture scale (ΔAdjusted R^2 = −0.0003), whereas the topographic component alone explained less variation than the traditional scale (ΔAdjusted R^2 = −0.0053). The combined CCA model including both edaphic and topographic moisture components explained a larger proportion of variation in species composition than either component alone (Adjusted R^2 = 0.0197). This value was nearly equal to the sum of the adjusted R^2 values obtained for the two single-component models (0.0124 + 0.0074 = 0.0198), indicating only limited overlap in their explanatory contributions. Although these contributions were statistically detectable, their absolute magnitude was small: the individual moisture scales accounted for only approximately 0.7–1.3% of community variation, while the combined edaphic–topographic model accounted for approximately 2%. The additional contribution of the topographic component should be interpreted as complementary but quantitatively modest.

3.6. Comparison of Moisture Indicator Scales with Environmental Moisture Gradients Across Spatial Validation Blocks

Spatially blocked assessment revealed a clear difference in the sensitivity of moisture indicator systems to the edaphic and topographic components of environmental moisture conditions (Table 3). Relationships with the raster-derived edaphic moisture gradient were generally more pronounced for the traditional and edaphic indicator scales than for the topographic scales. Among the traditional indicators, the Ellenberg scale exhibited the highest median block-specific correlation with EMI (median Spearman's ρ = 0.144), followed by the traditional Didukh scale (ρ = 0.092). The newly developed edaphic Didukh- and Ellenberg-based indicators showed weaker, but consistently positive, median associations (ρ = 0.064 and 0.053, respectively). In contrast, the topographic indicators showed essentially no systematic relationship with EMI (median ρ = 0.011 for the Didukh-based and −0.011 for the Ellenberg-based scale). The pooled correlations exhibited the same general pattern, with positive associations between EMI and the traditional and edaphic scales, whereas correlations with the topographic scales were close to zero. A contrasting pattern emerged for the topographic moisture gradient.

Table 3. Spatially blocked assessment of relationships between environmental moisture gradients and community-weighted phytoindication values.

Environmental Gradient	Phytoindication Scale	Median Spearman ρ (Q1–Q3)	Positive Blocks, n (%)	Pooled ρ
EMI (18 blocks)	Edaphic Didukh	0.064 (−0.084–0.258)	11 (61.1%)	0.135
	Edaphic Ellenberg	0.053 (−0.073–0.256)	11 (61.1%)	0.139
	Topographic Didukh	0.011 (−0.126–0.098)	10 (55.6%)	−0.003
	Topographic Ellenberg	−0.011 (−0.163–0.116)	8 (44.4%)	0.007
	Traditional Didukh	0.092 (−0.110–0.248)	10 (55.6%)	0.159
	Traditional Ellenberg	0.144 (−0.067–0.261)	11 (61.1%)	0.195
TMI (14 blocks)	Edaphic Didukh	−0.101 (−0.244–0.194)	6 (42.9%)	−0.141
	Edaphic Ellenberg	−0.108 (−0.269–0.191)	6 (42.9%)	−0.134
	Topographic Didukh	0.118 (−0.096–0.238)	9 (64.3%)	0.055
	Topographic Ellenberg	0.142 (−0.122–0.178)	9 (64.3%)	0.013
	Traditional Didukh	−0.070 (−0.183–0.182)	6 (42.9%)	−0.124
	Traditional Ellenberg	−0.074 (−0.187–0.168)	6 (42.9%)	−0.130

The newly developed topographic indicators were the only group showing positive median relationships with TMI, with median block-specific correlations of ρ = 0.118 for the Didukh-based scale and ρ = 0.142 for the Ellenberg-based scale. Positive relationships

occurred in nine of 14 spatial blocks (64.3%) for both topographic indicators. By comparison, the traditional and edaphic indicators showed negative median correlations with TMI, with positive relationships occurring in only six of 14 blocks (42.9%). Thus, the spatially blocked analysis indicates that the topographic indicators respond to a component of moisture variability that is poorly represented by conventional moisture indicator systems. The block-specific correlations varied substantially among geographical regions, indicating that the strength of vegetation–moisture relationships is spatially heterogeneous. The contrast between the two environmental gradients was consistent at the level of indicator groups: traditional moisture scales were more closely associated with the edaphic moisture component, whereas the topographic scales were specifically more responsive to topographically controlled moisture redistribution. These results support the interpretation of EMI and TMI as complementary rather than interchangeable dimensions of environmental moisture conditions and indicate that separating edaphic moisture availability from topographic moisture redistribution provides information not captured by conventional integrated moisture indicator scales.

3.7. Landscape-Level Comparison of Moisture Indicator Scales with Environmental Moisture Gradients

Three local landscape systems were used for landscape-level testing of the moisture indicator scales. The psammophytic steppe landscape was represented by 1079 vegetation plots comprising 299 vascular plant species. Species richness varied from 5 to 33 species per plot, with a mean of 13.4. NDWI values ranged from −0.197 to 0.556, and TWI values from 4.54 to 16.12. The floodplain ecosystem complex of Khortytsia Island included 878 vegetation plots and 333 vascular plant species. Species richness ranged from 6 to 30 species per plot, with a mean of 12.6. NDWI varied from −0.221 to 0.380, whereas TWI ranged from 3.94 to 17.40. The ravine–valley landscape system of Mayorka Valley was represented by 289 vegetation plots and 266 vascular plant species. This system showed the highest mean species richness, ranging from 8 to 40 species per plot, with a mean of 19.3. NDWI values ranged from 0.020 to 0.360, and TWI values from 1.26 to 13.99.

In the Mayorka Valley case study, relationships between SES and the TWI-predicted component of moisture differed substantially among the tested phytoindication scales (Figure 9). The strongest associations with topographically predicted moisture were observed for the newly developed topographic scales. The topographic scale based on the mean of extremes showed the highest explanatory power (R^2 = 0.276, RMSE = 0.80, MAE = 0.60), closely followed by the topographic optimum scale (R^2 = 0.249, RMSE = 0.94, MAE = 0.75). The traditional Didukh and Ellenberg scales exhibited considerably weaker relationships with TWI-predicted moisture (R^2 = 0.085 and 0.094, respectively), while the newly developed edaphic scales showed similarly low explanatory power (R^2 = 0.074–0.078). These results indicate that the proposed topographic indicators are substantially more sensitive to relief-controlled variation in moisture conditions than either the traditional phytoindication systems or the edaphic scales.

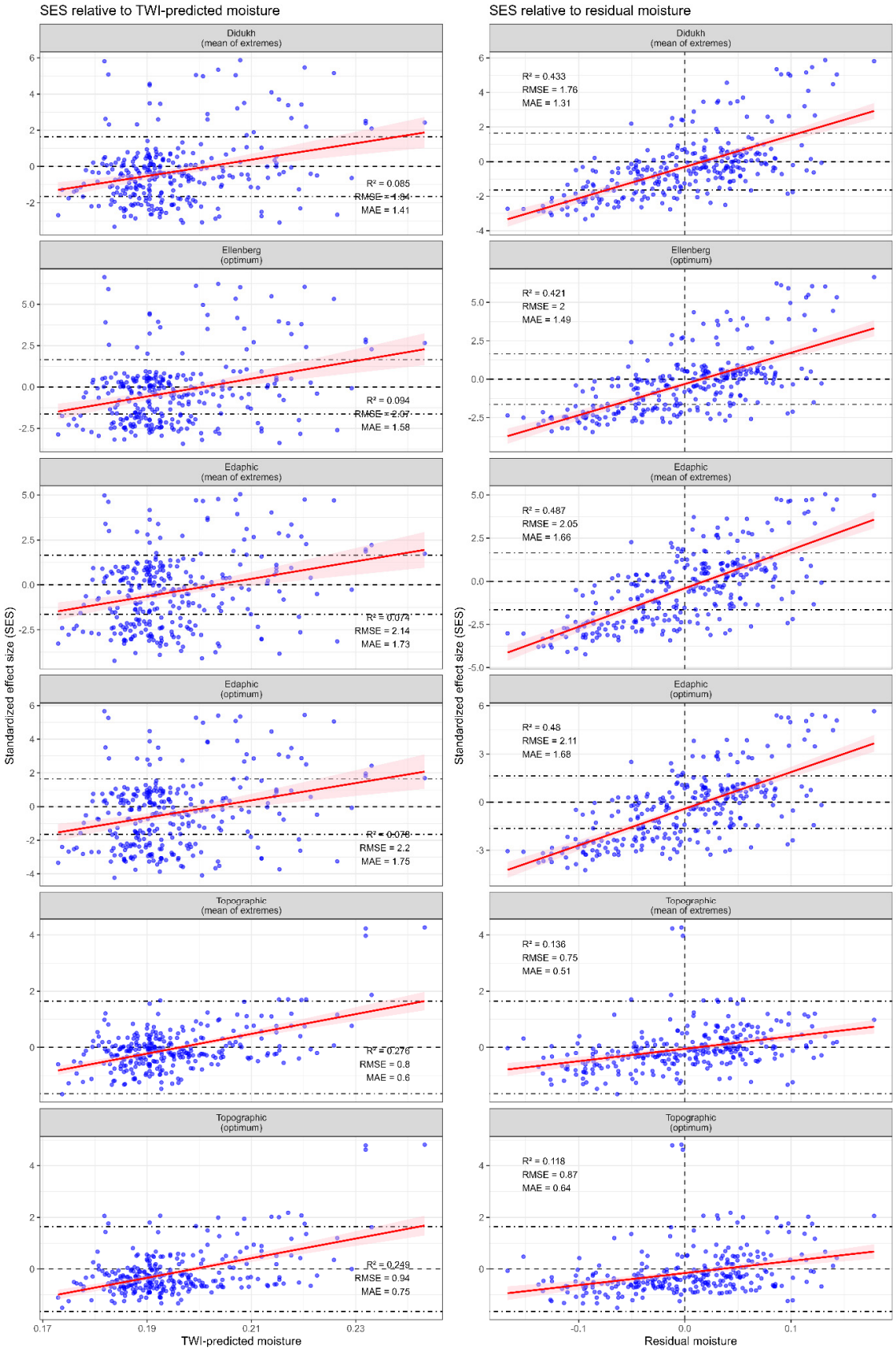


Figure 9. Relationships between standardized effect size (SES) and TWI-predicted moisture (**left**) and residual moisture (**right**) for different phytoindication moisture scales in the Mayorka Valley. Dashed and dot-dashed lines indicate SES thresholds used to define neutral and non-neutral observations. For each scale, the coefficient of determination (R^2), root mean square error (RMSE), and mean absolute error (MAE) are shown.

A contrasting pattern emerged for residual moisture, representing the component of moisture variation not explained by topography and therefore likely associated with local edaphic processes. In this case, the strongest relationships were observed for the edaphic scales (R^2 = 0.480–0.487), slightly exceeding those obtained for the traditional Didukh (R^2 = 0.433) and Ellenberg (R^2 = 0.421) scales. The topographic scales, by contrast, were only weakly related to residual moisture (R^2 = 0.118–0.136). Thus, the topographic indicators primarily captured the terrain-driven component of moisture variability, whereas the edaphic scales most effectively reflected the residual component of moisture conditions associated with local soil properties and microsite heterogeneity. Notably, most SES values remained within the neutral interval (−1.645 to 1.645), indicating that individual vegetation plots generally did not differ strongly from null-model expectations. Nevertheless, significant positive trends were observed along both the topographic and residual moisture gradients, suggesting that the ecological signal is expressed as a systematic directional shift in SES rather than as widespread strong deviations from the null expectation. This pattern implies that moisture gradients influence community assembly through cumulative changes in species composition, even when the majority of individual communities remain close to random expectations.

SES diagnostics were used to compare alternative phytoindication scales intended to characterize the same ecological dimension, namely moisture conditions. Within this framework, moisture indicator values were treated as functional traits of species, and the community-weighted mean indicator value was evaluated against a null model. Positive SES values indicated a non-random predominance of species with higher moisture indicator values within communities, whereas negative SES values indicated a non-random predominance of species with lower moisture indicator values. Thus, SES quantified departures of community-level moisture preferences from random expectation rather than patterns of trait dispersion. The Mayorka Valley data revealed remarkably similar patterns for the traditional and newly developed edaphic moisture indicators (Table 4).

Positive SES values accounted for 11.4% of observations for the Didukh scale, 12.1% for the Ellenberg scale, 13.5% for the edaphic mean-of-extremes scale, and 12.5% for the edaphic optimum scale. Negative SES values comprised 22.1%, 30.4%, 30.8%, and 31.1% of observations, respectively. Thus, the traditional and edaphic indicators exhibited broadly similar frequencies of significant positive and negative departures from null-model expectations. In contrast, approximately 98% of observations for the topographic indicators fell within the random expectation interval, while positive SES values accounted for only 1.4–1.7% of observations and negative SES values were absent. Relationships between positive SES values and the TWI-predicted moisture component were weak for all indicator scales, with slopes ranging from −0.05 to 0.33 for the traditional and edaphic indicators and from 0.09 to 0.29 for the topographic indicators. None of these slopes was statistically significant. A clearer pattern emerged for residual moisture. Significant positive slopes were observed for the Didukh, Ellenberg, and edaphic mean-of-extremes scales, with values ranging from 0.56 to 0.64. The edaphic optimum exhibited a larger but non-significant slope of 1.97. The topographic indicators showed negative slopes of −3.78 and −0.44, respectively, although neither relationship was statistically significant. These results indicate that departures from null-model expectations for the traditional and edaphic indicators were primarily structured along the residual moisture gradient, whereas the topographic indicators rarely exhibited significant SES deviations.

Table 4. SES diagnostics for phytoindication moisture scales.

Location	Parameter		Didukh (Mean of Extremes)	Ellenberg (Optimum)	Edaphic (Mean of Extremes)	Edaphic (Optimum)	Topographic (Mean of Extremes)	Topographic (Optimum)
Mayorka valley	Random expectation (%)		66.40	57.40	55.70	56.40	98.30	98.60
	Positive deviation from random expectation (%)		11.40	12.10	13.50	12.50	1.70	1.40
	Negative deviation from random expectation (%)		22.10	30.40	30.80	31.10	–	–
	TWI predicted	Positive SES slope	−0.00	−0.04	−0.05	0.33	0.29	0.09
		Negative SES slope	−0.04	−0.03	−0.03	–	–	–
	TWI residual	Positive SES slope	0.64	0.56	0.59	1.97	−3.78	−0.44
		Negative SES slope	0.08	0.15	0.14	–	–	0.02
Khortytsia Island	Random expectation (%)		79.30	72.90	79.60	74.30	97.00	94.90
	Positive deviation from random expectation (%)		15.80	22.00	15.50	20.50	1.70	4.00
	Negative deviation from random expectation (%)		4.90	5.10	4.90	5.20	1.30	1.10
	TWI predicted	Positive SES slope	−0.08	−0.01	0.01	−0.04	0.03	−0.01
		Negative SES slope	0.26	−0.03	0.24	0.19	−0.52	−0.10
	TWI residual	Positive SES slope	0.03	0.06	0.04	0.06	0.03	0.02
		Negative SES slope	0.25	0.08	0.12	0.08	0.19	0.16
The first above-floodplain terrace	Random expectation (%)		57.90	47.90	35.40	35.80	87.10	84.30
	Positive deviation from random expectation (%)		13.80	23.80	32.90	32.70	1.90	3.90
	Negative deviation from random expectation (%)		28.30	28.30	31.70	31.50	10.90	11.80
	TWI predicted	Positive SES slope	0.09	0.08	0.05	0.05	0.00	−0.02
		Negative SES slope	0.01	−0.02	−0.02	−0.02	−0.00	0.02
	TWI residual	Positive SES slope	0.24	0.21	0.05	0.07	−0.02	−0.19
		Negative SES slope	0.15	0.06	0.13	0.12	0.00	−0.09

In the floodplain ecosystems of Khortytsia Island, relationships between SES and TWI-predicted moisture were generally weak across all tested phytoindication scales (Figure 10). The highest explanatory power was observed for the Ellenberg optimum scale (R^2 = 0.107) and the edaphic optimum scale (R^2 = 0.110), whereas the Didukh and edaphic mean-of-extremes scales showed similarly weak associations (R^2 = 0.079 and 0.092, respectively). The topographic scales were only marginally related to TWI-predicted moisture (R^2 = 0.007 and 0.000). In contrast, substantially stronger relationships were observed for residual moisture, representing the component of NDWI variability not explained by TWI. The strongest responses were detected for the newly developed edaphic scales (R^2 = 0.259 and 0.265), followed by the Ellenberg (R^2 = 0.214) and Didukh (R^2 = 0.172) indicators. Topographic scales remained weakly related to residual moisture (R^2 = 0.051 and 0.037). This pattern indicates that moisture variation relevant for community assembly in the Khortytsia floodplain is driven primarily by edaphic and hydrological factors not captured by local TWI. The stronger performance of the regional edaphic scales suggests that their calibration improves the representation of moisture conditions operating in floodplain ecosystems.

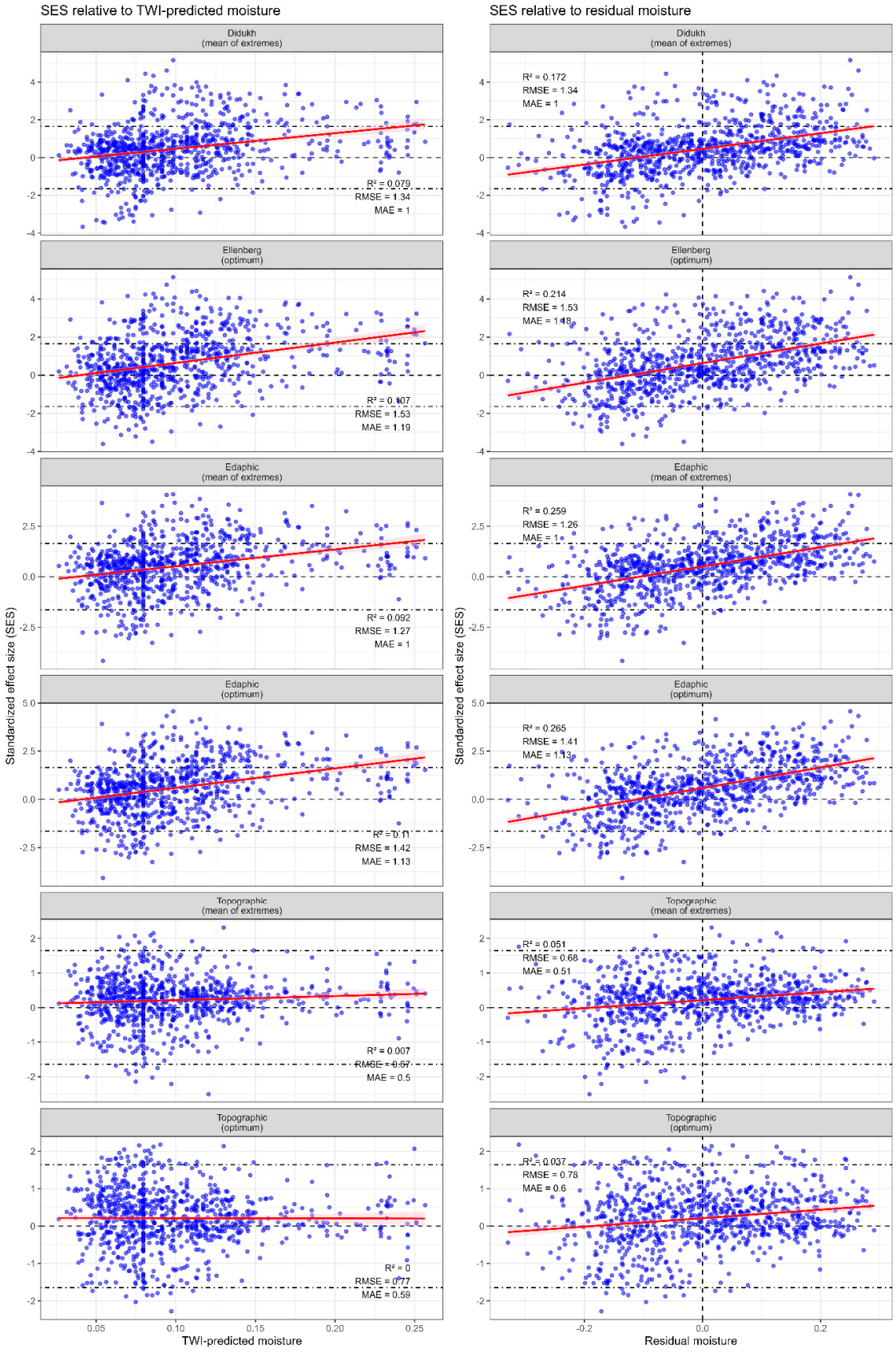


Figure 10. Relationships between standardized effect size (SES) and TWI-predicted moisture (**left**) and residual moisture (**right**) for different phytoindication moisture scales in the floodplain ecosystems of Khortytsia Island. Dashed and dot-dashed lines indicate SES thresholds used to define neutral and non-neutral observations. For each scale, the coefficient of determination (R^2), root mean square error (RMSE), and mean absolute error (MAE) are shown.

The SES diagnostics for the floodplain ecosystems of Khortytsia Island revealed a predominance of observations within the random expectation interval across all moisture indicators. Observations within the random expectation interval accounted for 72.9–97.0% of cases, whereas both positive and negative SES values occurred only infrequently. Positive SES observations were more frequent than negative SES observations for all indicators, but their proportions varied substantially among scales, ranging from 1.7–4.0% for the topographic scales to 15.5–22.0% for the phytoindication and edaphic scales. The Ellenberg optimum scale showed the highest proportion of positive SES observations (22.0%), followed by the edaphic optimum scale (20.5%), whereas the topographic scales were dominated by observations within the random expectation interval. This indicates that species-based moisture indicators more frequently produced significant positive departures from null-model expectations than purely topographic scales.

Relationships with the TWI-predicted component of moisture were generally weak. Slopes for plots with positive SES values were close to zero across all indicators, ranging from −0.08 to 0.03. Significant positive slopes for plots with negative SES values were observed for the Didukh scale (0.26), the edaphic mean-of-extremes scale (0.24), and the edaphic optimum scale (0.19), whereas the topographic mean-of-extremes scale showed a negative slope (−0.52). Residual moisture also produced weak responses among plots with positive SES values, although the edaphic optimum scale showed a small positive slope (0.06). Responses among plots with negative SES values were strongest for the Didukh scale (0.25), while the other indicators showed weaker positive slopes. The Khortytsia floodplain was characterized by a predominance of observations within the random expectation interval, with relatively few significant departures from the null model. The edaphic and traditional phytoindication scales were more responsive than the topographic scales, but the observed relationships remained modest, suggesting that community moisture patterns in these floodplain ecosystems reflect a complex hydrological regime that is only partly captured by TWI-derived moisture components.

In the sandy ecosystems of the first above-floodplain terrace of the Dnipro River, SES exhibited only weak relationships with the TWI-predicted component of moisture across all tested phytoindication scales (Figure 11). Coefficients of determination ranged from 0.030 to 0.050, indicating that topographically structured moisture variation explained only a small fraction of the observed variation in community assembly patterns. Even the newly developed topographic indicators showed only marginally stronger relationships than the traditional and edaphic scales. This pattern is consistent with the geomorphological setting of the sandy terrace, where relief is relatively subdued and local topographic redistribution of water contributes little to overall moisture heterogeneity. In contrast, SES was strongly associated with residual moisture, representing the component of moisture variation not explained by TWI and therefore likely linked to local edaphic conditions. Very high coefficients of determination were observed for the traditional and edaphic moisture indicators. The Didukh and Ellenberg scales yielded R^2 values of 0.812 and 0.793, respectively, while the newly developed edaphic mean-of-extremes and optimum scales showed the strongest relationships overall (R^2 = 0.834 and 0.833).

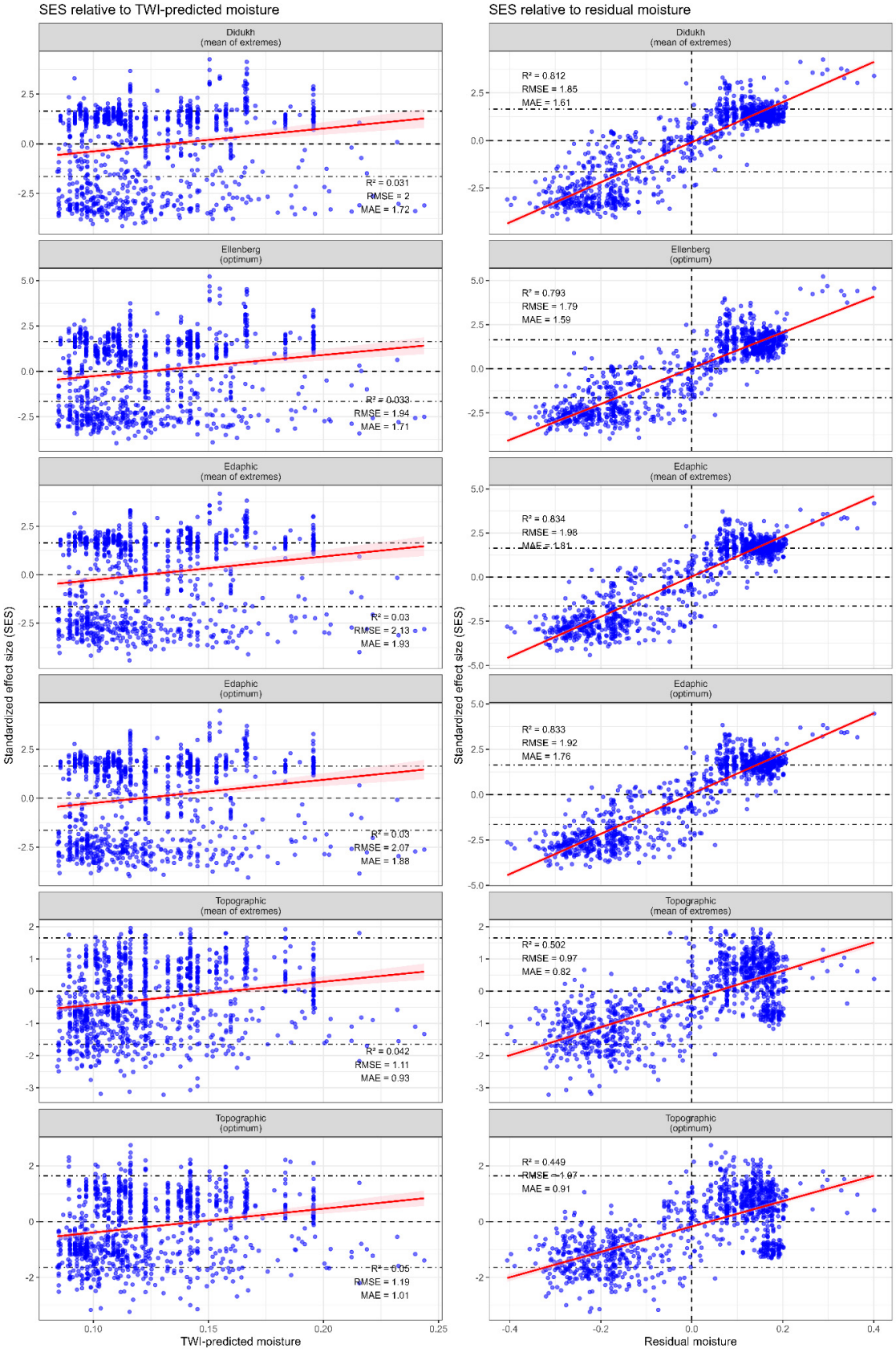


Figure 11. Relationships between standardized effect size (SES) and TWI-predicted moisture (**left**) and residual moisture (**right**) for different phytoindication moisture scales in the sandy ecosystems of the first above-floodplain terrace of the Dnipro River. Dashed and dot-dashed lines indicate SES thresholds used to define neutral and non-neutral observations. For each scale, the coefficient of determination (R^2), root mean square error (RMSE), and mean absolute error (MAE) are shown.

The near-identical responses of these four indicators suggest that they capture the same dominant environmental gradient governing community assembly in the sandy terrace ecosystems. The topographic indicators behaved differently. Although they also responded positively to residual moisture, their explanatory power was substantially lower (R^2 = 0.502 for the mean-of-extremes scale and R^2 = 0.449 for the optimum scale) than that of the traditional and edaphic indicators. Thus, while the topographic scales retain some sensitivity to moisture variation, they provide a less accurate representation of the principal moisture gradient operating in these ecosystems. The results indicate that moisture-related community assembly on the sandy terrace is governed predominantly by edaphic rather than topographic controls. The weak relationships with the TWI-predicted component and the consistently strong relationships with residual moisture suggest that local soil properties, rather than terrain-driven water redistribution, constitute the primary mechanism structuring moisture-related variation in plant communities.

The SES diagnostics for the sandy ecosystems of the first above-floodplain terrace revealed clear differences between the traditional and edaphic moisture indicators on the one hand and the topographic indicators on the other (Table 4). The traditional and edaphic scales showed broadly similar patterns of departures from null-model expectations. Observations within the random expectation interval accounted for 35.4–57.9% of cases, whereas positive SES values comprised 13.8–32.9% and negative SES values 28.3–31.7%. The newly developed edaphic indicators exhibited the highest proportions of both positive (32.7–32.9%) and negative (31.5–31.7%) SES values, indicating a high sensitivity to non-random variation in community-level moisture indicator values. The Didukh scale yielded the lowest proportion of positive SES observations (13.8%), whereas the Ellenberg scale occupied an intermediate position (23.8%). In contrast, the topographic indicators were dominated by observations within the random expectation interval, accounting for 84.3–87.1% of cases. Positive SES values were rare (1.9–3.9%), and negative SES values remained comparatively infrequent (10.9–11.8%). Thus, the topographic indicators detected substantially fewer significant departures from null-model expectations than either the traditional or the edaphic moisture scales. The TWI-predicted moisture component exhibited only weak relationships with SES patterns. Positive slopes for plots with positive SES values were observed for the Didukh (0.09), Ellenberg (0.08), and both edaphic scales (0.05), whereas the topographic indicators showed slopes close to zero (0.00 and −0.02). Slopes for plots with negative SES values were negligible for all indicators (−0.02 to 0.02). These results suggest that topographically structured moisture variation contributes little to departures from random expectation in the sandy terrace ecosystems. A much stronger pattern emerged for residual moisture. Positive slopes for plots with positive SES values were observed for all traditional and edaphic indicators, reaching 0.24 for the Didukh scale and 0.21 for the Ellenberg scale, compared with 0.05 and 0.07 for the edaphic mean-of-extremes and optimum scales, respectively. Positive slopes for plots with negative SES values were also detected for these indicators, ranging from 0.06 to 0.15. In contrast, the topographic indicators showed little response to residual moisture, with slopes close to zero or slightly negative.

Empirical variograms revealed spatial dependence in both measured soil moisture and TWI, although the estimated autocorrelation ranges differed substantially among landscapes and between the two variables (Figure S1; Table S6). For measured soil moisture, the best-fitting variogram model was exponential in Khortytsia and Mayorka and Gaussian in the Psammophytic steppe. The corresponding effective ranges were 568, 243, and 140 m, respectively, indicating a progressive decrease in the characteristic spatial scale of measured moisture variation across these three landscapes. TWI showed a different pattern. Its effective autocorrelation range was relatively short in Khortytsia

(222 m; spherical model), but considerably larger in Mayorka (1658 m) and the Psammophytic steppe (1077 m), where Gaussian models provided the best fits. Thus, the spatial scale of autocorrelation was landscape- and variable-specific, and the spatial structure of measured soil moisture did not simply reproduce that of TWI. The landscape-specific effective ranges of measured soil moisture were subsequently used to define spatial dependence units for spatially blocked validation. Based on the landscape-specific autocorrelation ranges, the sampling plots were partitioned into 34 spatial dependence units in Khortytsia, 50 in Mayorka, and 146 in the Psammophytic steppe. These units were subsequently grouped into five spatial validation folds within each landscape (Figure S2). The resulting folds preserved the spatially aggregated structure of the sampling designs while separating groups of spatially dependent plots among validation subsets. Fold sizes ranged from 66 to 370 plots in Khortytsia, from 30 to 84 plots in Mayorka, and from 46 to 589 plots in the Psammophytic steppe. Thus, all three landscape datasets could be partitioned into five spatial validation subsets without splitting the spatial dependence units defined from the estimated autocorrelation ranges. This spatial partitioning was subsequently used to evaluate the stability of the relationships between measured soil moisture and phytoindication estimates and of the SES-based diagnostics.

Spatially blocked SES diagnostics were broadly consistent across the five validation folds (Table S7). The relative prevalence of the three SES categories was retained across spatial subsets, although their proportions differed markedly among landscapes and phytoindication scales. Khortytsia was predominantly characterized by values within random expectation, whereas below-random values were consistently more frequent in the Psammophytic steppe, particularly for the Didukh, Ellenberg, and edaphic scales. Mayorka showed an intermediate pattern, while the topographic scales were dominated by values within random expectation. Thus, the principal SES patterns were consistently reproduced across spatial validation folds rather than being attributable to a particular spatial subset of plots. This spatial consistency was also supported by fold-specific Spearman correlations between measured soil moisture and phytoindication estimates (Table S8). Correlations were positive in all five folds for all scales in Mayorka and the Psammophytic steppe and for the Didukh, Ellenberg, and edaphic scales in Khortytsia. Median correlations ranged from 0.414 to 0.631 in Mayorka and from 0.223 to 0.712 in the Psammophytic steppe. In Khortytsia, the Didukh, Ellenberg, and edaphic scales showed consistently positive relationships (ρ = 0.384–0.573), whereas correlations for the topographic scales were weaker and positive in four of five folds. Together, the SES diagnostics and rank-correlation analysis indicate that the main patterns were robust to spatial partitioning of the three landscape datasets.

3.8. Assessment of Ecological Consistency of Moisture Indicator Scales

All analysed moisture scales showed a mutually consistent ordering of species moisture preferences, including the continuous traditional and newly developed phytoindication scales as well as the categorical-ordinal Belgard–Tarasov hygromorph classification (Figure 12). The newly developed edaphic moisture scales exhibited the strongest correspondence with the independent Belgard–Tarasov hygromorph classification (ρ = 0.69–0.70). Their correlations exceeded those observed for the traditional Ellenberg optimum scale (ρ = 0.66) and the Didukh minimum and maximum moisture values (ρ = 0.59–0.64). In contrast, the topographic moisture scales showed substantially weaker associations with the hygromorph score (ρ = 0.22–0.30). These results indicate that the edaphic scales most closely reproduce expert assessments of species moisture preferences, whereas the topographic scales represent a distinct moisture-related dimension that is only weakly reflected in the traditional hygromorph classification.

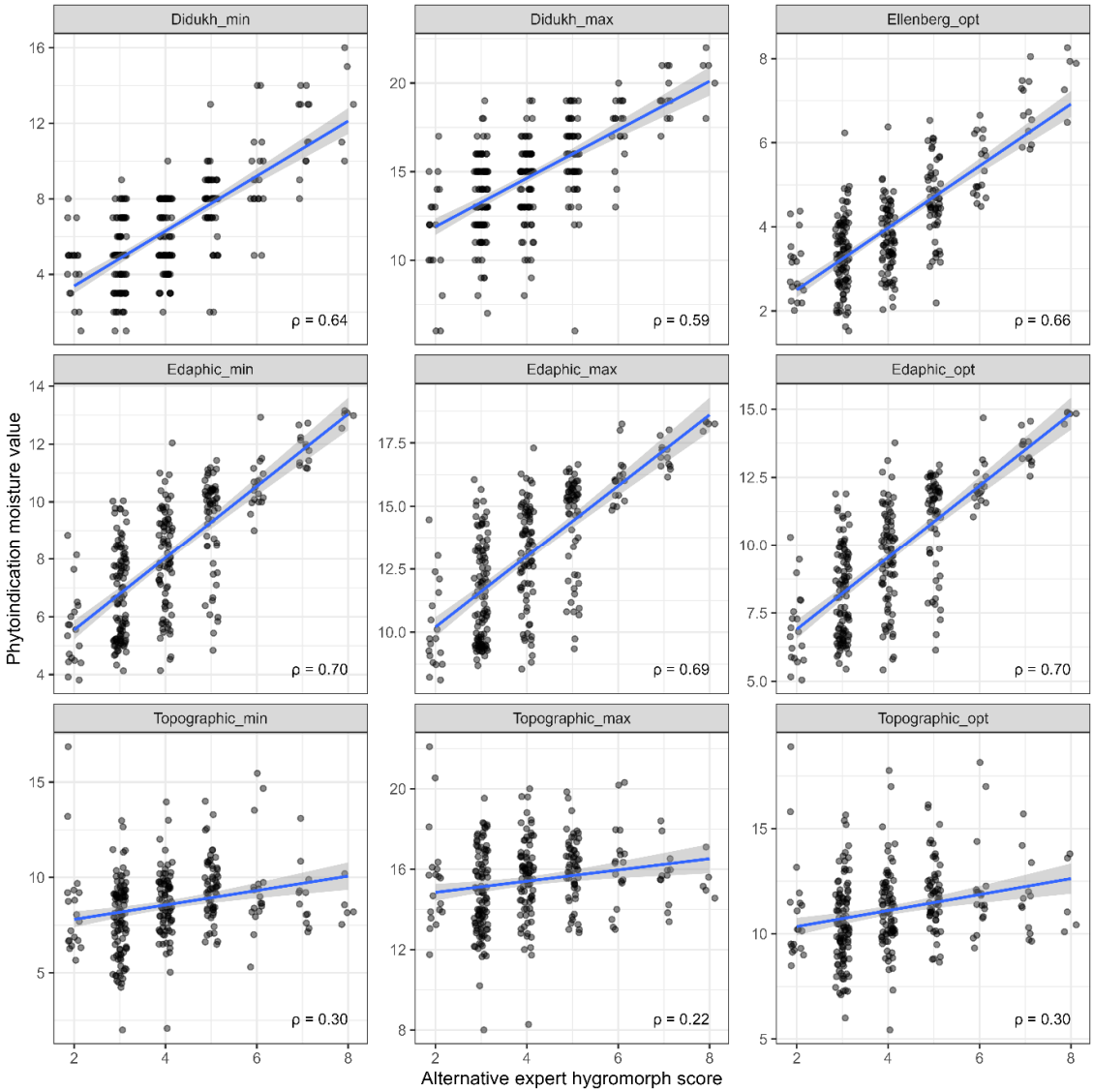


Figure 12. Relationships between Belgard–Tarasov hygromorph categories and phytoindication moisture scales. Species-level moisture indicator values are plotted against the alternative expert hygromorph scores. The Belgard–Tarasov hygromorph classes are ordered from 2 to 8: 2—Xero, xerophyte; 3—MsXero, meso-xerophyte; 4—XeroMs, xero-mesophyte; 5—Ms, mesophyte; 6—HgMs, hygro-mesophyte; 7—MsHg, meso-hygrophyte; 8—Hg, hygrophyte. Blue lines represent linear regression fits with 95% confidence intervals. Spearman's rank correlation coefficient (ρ) is shown in each panel.

4. Discussion

4.1. Edaphic and Topographic Components of the Moisture Regime

The most important outcome of this study is the evidence that the ecologically relevant moisture regime in the steppe zone of Ukraine cannot be adequately described by a single moisture gradient. Analysis of species distributions revealed the existence of at least two complementary dimensions of moisture availability, each showing a different pattern of association with environmental controls governing the formation of the water regime. Both dimensions were consistently associated with the climatic precipitation gradient, confirming the fundamental role of atmospheric water supply as the primary source of moisture for terrestrial ecosystems. However, the subsequent fate of this water is determined by different environmental processes. The first dimension was primarily associated with soil texture and its water-retention capacity. This finding is consistent with

the widely accepted view that soil physical properties, particularly soil texture, are among the principal drivers of soil moisture dynamics because they regulate water retention, infiltration, hydraulic conductivity, and the amount of water available to plants [79]. It should be noted that soil texture also serves as a proxy for the variability of several other soil properties that collectively determine water-holding capacity, including organic matter content, soil profile depth, aggregate structure, bulk density, and related characteristics [80]. This gradient, therefore, reflects the contrast between substrates with high water-storage capacity and coarse-textured sandy soils, where water is rapidly lost through infiltration or evaporation. The traditional phytoindication moisture scales proved to be primarily sensitive to this component of the moisture regime. This finding suggests that the edaphic component of moisture availability most likely represents the aspect of the water regime that historically underpinned expert assessments of species ecological optima and tolerance ranges. The second dimension was associated predominantly with topographically driven water redistribution. It characterises the contrast between landscape positions that favour water accumulation and those dominated by drainage and runoff. Unlike the edaphic component, this gradient is only weakly captured by traditional phytoindication systems, although the present results demonstrate that it makes a complementary contribution to plant community assembly. Recent studies have shown that similar climatic conditions may lead to different levels of ecosystem water availability because soil hydraulic properties strongly modulate the onset of water limitation [79]. Moreover, the relationship between precipitation and soil moisture is spatially heterogeneous and non-linear, being shaped not only by rainfall input but also by evapotranspiration, vegetation type, runoff, and soil properties [81]. The present findings extend this view by showing that plant communities respond differentially to the edaphic and topographic components of the moisture regime. Consequently, identical levels of climatic water input may yield different ecological outcomes. Under the same precipitation regime, plant communities may develop either on soils differing in water-retention capacity or on topographic surfaces with contrasting patterns of water redistribution. These findings indicate that moisture, as an ecological factor, is inherently multidimensional and that its representation by a single integrated gradient inevitably obscures part of the ecologically meaningful variation governing plant community composition.

4.2. Why Topographic Moisture Is Underrepresented in Traditional Phytoindication Scales

A key finding of this study is the asymmetric contribution of the two identified components of the water regime. The edaphic component explained a larger proportion of variation in plant responses and showed a close relationship with traditional phytoindication scales. The topographic component was also statistically significant, but its contribution was smaller and, more importantly, substantially more context-dependent. Unlike soil texture, which is a relatively stable property of a habitat, the effect of relief on the moisture regime is mediated by water redistribution processes whose intensity depends on weather conditions, precipitation amount and seasonality, and the spatial scale of analysis [82]. This interpretation is consistent with studies showing that topographic controls on soil moisture are state-dependent rather than constant [82]. The ecological effect of topographic water accumulation or drainage is not invariant [83,84], providing a mechanistic explanation for our finding that the same landform element may promote moisture accumulation under some hydrological conditions but have little effect, or even function primarily as a drainage pathway, under others. This context dependence probably explains why the topographic component is only weakly reflected in traditional phytoindication systems. Phytoindication scales are constructed as generalisations of stable patterns in species' ecological behaviour over broad geographical ranges. Such generalisations naturally emphasise the most stable

components of the environment, primarily those related to the substrate's water-retention capacity and the overall climatic moisture supply. By contrast, topographically driven variability is local in character and depends on the specific combination of climatic, geomorphological, and hydrological conditions. As a result, its signal is partly lost during the construction of generalised species-specific indicator values.

4.3. Phytoindication Reflects Realised Ecological Moisture Conditions Rather than Single Hydrological Variables

The present results are fully consistent with previous studies demonstrating that the predictive value of TWI and phytoindication estimates increases substantially when information on soil water-holding capacity is incorporated. In particular, previous studies have demonstrated that adding soil water capacity as an additional predictor increases the explanatory power of both TWI-based and Ellenberg indicator value-based models of soil moisture conditions, with a particularly pronounced improvement for Ellenberg values [32]. This finding highlights the fundamental ecological importance of soil texture and related soil properties as determinants of the amount of water available to plants after precipitation events and topographic redistribution processes. The results obtained in the present study provide a conceptual explanation for this pattern. The analysis revealed that the dominant component of the moisture gradient perceived by vegetation is associated with the soil-mediated capacity of ecosystems to retain water, whereas topographic controls represent a secondary and more context-dependent source of variation. Consequently, information on soil texture contributes substantially to the ecological interpretation of moisture conditions beyond that provided by climatic or topographic variables alone. These findings also emphasise an important distinction between phytoindication and direct environmental measurements. The primary purpose of phytoindication is not to quantify moisture itself, but to characterise the biological response of vegetation to moisture conditions [23]. From this perspective, disagreement between phytoindication estimates and individual environmental variables should not necessarily be interpreted as a limitation of phytoindication. Rather, it reflects the fact that plant communities respond to the integrated effects of multiple environmental controls, including climatic inputs, soil water retention, groundwater influence, and topographic redistribution. Phytoindication, therefore, provides information on the realised ecological consequences of the water regime rather than on any single component of the hydrological system.

TMI should not be interpreted as a transformed version of TWI. TWI represents the topographic potential for water accumulation based on terrain configuration, whereas TMI represents the empirically observed vegetation response to topographically mediated water redistribution in interaction with climatic and edaphic conditions. Consequently, a high TWI does not necessarily imply a proportionally high TMI. The positive precipitation $\times$ TWI interaction indicates that the ecological effect of topographic accumulation increases with climatic water supply, whereas the negative conditional TWI effect indicates that topographic accumulation potential may overestimate realised moisture availability under some environmental conditions. Such decoupling may occur, for example, on highly permeable sandy substrates, where water delivered to topographically favourable positions can percolate below the root-accessible soil layer rather than remain available to vegetation.

4.4. An Ecological Framework for Integrating Multiple Determinants of the Moisture Regime

A central contribution of this study is the demonstration that multiple abiotic determinants of the water regime can be integrated into ecologically meaningful moisture indices using vegetation itself as the calibration target. Previous approaches have generally considered climatic water supply, soil water-holding capacity, and topographic redistribution as independent components of the hydrological system [85,86]. In contrast, our

approach integrates these processes within a single ecological framework by using plant community responses to identify the combinations of abiotic factors that best represent realised moisture conditions. An equally important distinction from traditional climatic moisture coefficients is that the proposed indices are not based solely on physical assumptions about the hydrological cycle. Instead, their mathematical structure was empirically calibrated against vegetation responses inferred from millions of species occurrence records and established phytoindication systems. Consequently, the regression coefficients represent empirically derived ecological relationships rather than predefined physical weights, allowing the indices to quantify moisture conditions in terms of their biological relevance for plant communities rather than only their physical hydrological characteristics.

A further important feature of the proposed indices is that they explicitly include interaction terms among the principal predictors. This is ecologically essential because precipitation, TWI, and soil texture do not independently affect plant-available moisture. The same amount of precipitation may have very different ecological consequences depending on whether it falls on coarse- or fine-textured soils and whether a site is on a drained slope, a flat surface, or a topographically convergent position. Similarly, the effect of topographic water accumulation depends on the soil's capacity to retain this water and on the broader climatic context in which redistribution occurs. Such interactions are intuitively expected but difficult to derive analytically. The response of vegetation to the moisture regime is mediated by multiple processes, including infiltration, runoff, capillary rise, evaporation, soil water retention, rooting depth, and species-specific tolerance ranges. These processes are non-linear, scale-dependent, and partly compensatory. Therefore, a purely theoretical formulation of the combined effect of precipitation, relief, and soil texture would inevitably require strong simplifying assumptions. In this respect, the empirical approach used here provides a practical solution: it allows the interaction structure among abiotic predictors to be estimated directly from the realised vegetation response. The resulting formulae should not be interpreted simply as algebraic combinations of environmental variables. Rather, they represent empirically calibrated ecological summaries of how climatic water input, topographic redistribution, and soil-mediated retention jointly shape the moisture conditions experienced by plant communities. The inclusion of interaction terms is therefore not only a statistical refinement but also a necessary ecological component of the model. It reflects the fact that plant-available moisture arises from the combined, context-dependent action of several environmental controls, rather than from their additive effects alone.

4.5. Future Applications of Edaphic and Topographic Moisture Indices in Spatial Mapping and Environmental Assessment

An important potential application of the proposed indices is the production of spatially explicit representations of moisture-regime variability based on abiotic predictors. By applying the fitted formulae to raster layers of precipitation, TWI, and soil texture, the proposed framework opens prospects for mapping edaphic and topographic components of moisture conditions across large territories. This approach supports ecological interpretation, vegetation analysis, and regional environmental assessment by translating separate climatic, geomorphological, and soil variables into ecologically calibrated moisture gradients. The significance of this approach extends beyond the current mapping of moisture conditions. It is also important for forecasting vegetation responses under climate change [87]. In most climate-change scenarios, precipitation is usually treated as the primary variable component of the water regime [88–90]. Yet changes in precipitation will not be translated into plant-available moisture uniformly across landscapes. The same climatic shift may produce different ecological consequences depending on local soil texture, water-retention capacity, and topographic position. Areas with fine-textured soils may buffer short-term reductions in precipitation more effectively than sandy substrates,

while topographically convergent positions may retain or accumulate water even under drier regional conditions. Conversely, well-drained slopes and coarse-textured soils may experience stronger ecological drying under the same climatic scenario. The projections of future moisture conditions should not be based solely on precipitation changes. The real ecological effect of climate change on vegetation moisture regimes must be interpreted in the context of relief and soil properties. The proposed edaphic and topographic indices can be considered as a practical framework for such interpretation. They may facilitate the translation of changes in climatic water input into spatially differentiated estimates of ecologically relevant moisture availability, accounting for both soil capacity to retain water and terrain capacity to redistribute it. This makes the indices potentially useful not only for present-day mapping but also for scenario-based assessment of future changes in plant habitats and vegetation structure.

4.6. Robustness of Traditional Phytoindication Scales and the Limited Effect of Local Recalibration

Local recalibration of indicator scales can improve their ecological performance, but the magnitude of this improvement is not large. The newly derived edaphic scale showed slightly higher consistency across several complementary assessments, including reduced within-community variation for some moisture parameters, stronger correspondence with the Belgard–Tarasov hygromorph classification, and clearer differentiation of residual moisture gradients in local landscapes. However, these advantages were moderate rather than radical. In many cases, the traditional Didukh and Ellenberg moisture scales performed similarly to the locally calibrated edaphic scale. This result is important because it does not indicate a weakness of the traditional phytoindication systems. On the contrary, it confirms their broad ecological robustness. Despite being developed on the basis of expert knowledge and regional floristic experience, the Didukh and Ellenberg scales captured the dominant edaphic component of moisture variability over a wide geographical and ecological range. Therefore, local recalibration may be useful when higher spatial resolution or specific regional interpretation is required, but the traditional scales remain reliable tools for general ecological assessment. Thus, the proposed approach should be regarded not as a replacement for established phytoindication systems, but as a means of refining and decomposing them. It helps clarify which component of the moisture regime is primarily represented by traditional scales and where additional information can be obtained from locally calibrated or topographic indicators. The limited magnitude of improvement also supports the continued use of Didukh and Ellenberg indicator values in broad-scale vegetation studies, especially where direct recalibration is not possible or where comparability across regions is required.

4.7. Ecological Mechanisms Behind Phytoindication Performance

An important aspect of our results concerns the ecological mechanism underlying the indicator value of plant communities. The widespread use of phytoindication has been accompanied by the concern that its predictive performance may sometimes appear "too good to be true", because indicator values and community composition are not statistically independent. Zelený and Schaffers [91] demonstrated that part of this apparent explanatory power stems from compositional similarity, rather than from environmental responses, and proposed randomisation procedures to separate these effects. Our randomisation analyses suggest that the ecological information represented by alternative moisture indicator scales differs substantially. The traditional phytoindication scales and the newly developed edaphic indicators frequently exhibited significant departures from null-model expectations, whereas the topographic indicators were dominated by observations consistent with random expectation. This contrast indicates that species-based and terrain-based indicators

characterize different components of the moisture regime. Consequently, phytoindication reflects not only variation in environmental moisture conditions but also non-random patterns of community composition associated with those conditions.

According to this criterion, the traditional Didukh and Ellenberg scales consistently exhibited a high proportion of significant departures from null-model expectations, confirming their suitability as indicators of realised moisture conditions. The locally recalibrated edaphic scale performed slightly better, suggesting that local calibration increases the ecological signal associated with community-level moisture conditions. In contrast, the topographic moisture indicator exhibited a context-dependent pattern. In most communities, its SES values remained within the range expected under the null model, whereas significant positive or negative departures occurred only under particular environmental conditions. This behaviour is consistent with the indirect nature of topographic controls, which influence plant water availability through interactions with soil properties, hydrological connectivity, and local landscape configuration, rather than acting as direct ecological factors themselves.

5. Conclusions

This study empirically derived calibrated moisture indices that integrate climatic, edaphic, and topographic determinants of the water regime through the realised response of vegetation. These indices combine climatic water supply, soil water-retention properties, and topographic redistribution into comprehensive descriptors of the moisture conditions experienced by plant communities. The proposed indices were calibrated against the actual ecological responses of vegetation, thereby quantifying moisture conditions not only in physical terms but also in terms of their biological relevance to plants. The importance of interaction terms indicates that vegetation responses to moisture are better described by models allowing non-additive effects of precipitation, soil properties, and topographic context. As such interactions arise from coupled hydrological and ecological processes, they are effectively captured through empirical calibration. The resulting framework identifies complementary edaphic and topographic components of realised moisture conditions within the adopted modelling framework. While both indices describe realised moisture conditions, they differ in their ecological interpretation and spatial behaviour, providing complementary perspectives on moisture-related variation in plant communities.

Supplementary Materials: The following supporting information can be downloaded at: https://www.mdpi.com/article/10.3390/d18090507/s1, Figure S1: Empirical variograms and fitted variogram models for measured soil moisture and topographic wetness index (TWI) in the three local landscape datasets. Empirical semivariance is shown as a function of spatial distance for the Khortytsia, Mayorka, and Psammophytic steppe datasets. Solid lines represent the best-fitting theoretical variogram models selected among spherical, exponential, and Gaussian models. The fitted models were used to estimate the effective range of spatial autocorrelation for subsequent definition of spatial dependence units and spatially blocked validation; Figure S2: Spatially blocked validation design for the three local landscape datasets. Sampling plots in the Khortytsia, Mayorka, and Psammophytic steppe datasets were assigned to five spatial validation folds based on spatial dependence units defined using the estimated range of spatial autocorrelation. Different colours indicate the five spatial validation folds used to assess the robustness of relationships between phytoindication estimates and measured environmental conditions while accounting for spatial dependence; Table S1: Sensitivity of sampling support and species–environment matrix structure to environmental discretization resolution; Table S2: Stability of the constrained CCA ordination across alternative environmental discretization schemes. The 27 models represented all factorial combinations of 5, 10, and 15 bins for precipitation, TWI, and soil texture. Procrustes correlations were calculated for species configurations relative to the 15 × 15 × 10 ordination; Table S3: Sensitivity of constrained ordination

to alternative weighting of species occurrence records; Table S4: Sensitivity of the CCA ordination to unequal environmental availability. Environmental availability was estimated as the proportional area occupied by each environmental supercluster within the European raster domain. CCA1–CCA3 are expressed as percentages of total constrained inertia. Procrustes *r* measures congruence of species configurations with the uncorrected CCA solution. Dominant associations indicate the environmental predictor showing the highest absolute Spearman correlation with the corresponding CCA site scores; Table S5: Sensitivity of the CCA ordination to GBIF spatial sampling intensity. CCA1–CCA3 are expressed as percentages of total constrained inertia. Procrustes *r* represents congruence of species configurations with the 10-km thinning solution. Dominant associations correspond to the environmental variable with the largest absolute Spearman correlation with the respective CCA site scores; Table S6: Variogram models and estimated spatial autocorrelation ranges across the three landscape datasets. Effective range was taken as the fitted range for the spherical model, 3 × the fitted range for the exponential model, and $\sqrt{3}$ × the fitted range for the Gaussian model. SSE denotes the residual sum of squares of the fitted variogram model; Table S7: Spatial stability of SES-based diagnostics across five spatial folds in three landscape datasets. Values are medians [Q1–Q3] across five spatial folds. "Within random expectation" denotes, "above random expectation" denotes, and "below random expectation" denotes. An em dash indicates that the corresponding category was absent across all five folds; Table S8: Spatially blocked Spearman correlations across three landscape datasets. Values are medians [Q1–Q3] of fold-specific Spearman rank correlations across five spatial folds. Positive folds indicate the number of folds with $\rho > 0$.

Author Contributions: Conceptualization, O.K. and O.Z.; methodology, O.L.; software, H.T.; validation, O.K., O.L. and O.Z.; formal analysis, H.T.; investigation, O.L.; resources, O.Z.; data curation, H.T.; writing—original draft preparation, O.Z.; writing—review and editing, O.K.; visualization, O.L.; supervision, H.T.; project administration, O.L.; funding acquisition, O.Z. All authors have read and agreed to the published version of the manuscript.

Funding: This research was funded by the National Research Foundation of Ukraine, grant number 2025.07/0001, "Procrustean analysis of spectral indices for assessing changes in hemeroby and the functional structure of plant communities as a result of military destruction: the example of the destruction of the Kakhovka Reservoir".

Data Availability Statement: The primary datasets used in this study are publicly available through the Global Biodiversity Information Facility (GBIF) and Zenodo, with the corresponding dataset citations and persistent identifiers provided in the methods and references. The results of the sensitivity analyses and spatial validation are provided in the Supplementary Materials. The R scripts used for the principal analyses are available from the corresponding author upon reasonable request.

Acknowledgments: The authors would like to express their sincere gratitude to the leadership of Bohdan Khmelnytskyi Melitopol State Pedagogical University for their administrative and technical support. The authors have reviewed and edited the output and take full responsibility for the content of this publication. We are also grateful to the staff of the National Nature Reserve "Khortytsia" for their assistance in conducting field studies and for ensuring the safety of fieldwork under the challenging conditions of ongoing hostile UAV attacks.

Conflicts of Interest: The authors declare no conflicts of interest.

References

1. Albertson, J.D.; Montaldo, N. Temporal Dynamics of Soil Moisture Variability: 1. Theoretical Basis. *Water Resour. Res.* **2003**, *39*, 1274. [CrossRef]
2. Jach, L.; Fluhrer, A.; Bauer, H.-S.; Chaparro, D.; Hellwig, F.M.; Portal, G.; Jagdhuber, T. Comparing Temporal Dynamics of Soil Moisture from Remote Sensing, Modeling, and Field Observations Across Europe. *Remote Sens.* **2026**, *18*, 445. [CrossRef]
3. Ricks, K.D.; Yannarell, A.C. Soil Moisture Incidentally Selects for Microbes That Facilitate Locally Adaptive Plant Response. *Proc. R. Soc. B Biol. Sci.* **2023**, *290*, 20230469. [CrossRef]
4. Milici, V.R.; Ballesteros, J.; Bagchi, R. High Soil Moisture Triggers Negative Plant–Soil Feedbacks in a Tropical Forest. *Funct. Ecol.* **2025**, *39*, 1469–1482. [CrossRef]

5. Stefan, G.; Cornelia, B.; Jörg, R.; Michael, B. Soil Water Availability Strongly Alters the Community Composition of Soil Protists. *Pedobiologia* **2014**, *57*, 205–213. [CrossRef]
6. Fatichi, S.; Katul, G.G.; Ivanov, V.Y.; Pappas, C.; Paschalis, A.; Consolo, A.; Kim, J.; Burlando, P. Abiotic and Biotic Controls of Soil Moisture Spatiotemporal Variability and the Occurrence of Hysteresis. *Water Resour. Res.* **2015**, *51*, 3505–3524. [CrossRef]
7. Johnson, W.M.; Niederhof, C.H. Some Relationships of Plant Cover to Run-off, Erosion, and Infiltration on Granitic Soils. *J. For.* **1941**, *39*, 854–858. [CrossRef]
8. Boyle, M.; Frankenberger, W.T.; Stolzy, L.H. The Influence of Organic Matter on Soil Aggregation and Water Infiltration. *J. Prod. Agric.* **1989**, *2*, 290–299. [CrossRef]
9. Xiao, T.; Li, P.; Fei, W.; Wang, J. Effects of Vegetation Roots on the Structure and Hydraulic Properties of Soils: A Perspective Review. *Sci. Total Environ.* **2024**, *906*, 167524. [CrossRef]
10. Cerdà, A. Effects of Rock Fragment Cover on Soil Infiltration, Interrill Runoff and Erosion. *Eur. J. Soil Sci.* **2001**, *52*, 59–68. [CrossRef]
11. Seneviratne, S.I.; Corti, T.; Davin, E.L.; Hirschi, M.; Jaeger, E.B.; Lehner, I.; Orlowsky, B.; Teuling, A.J. Investigating Soil Moisture–Climate Interactions in a Changing Climate: A Review. *Earth-Sci. Rev.* **2010**, *99*, 125–161. [CrossRef]
12. Vereecken, H.; Schnepf, A.; Hopmans, J.W.; Javaux, M.; Or, D.; Roose, T.; Vanderborght, J.; Young, M.H.; Amelung, W.; Aitkenhead, M.; et al. Modeling Soil Processes: Review, Key Challenges, and New Perspectives. *Vadose Zone J.* **2016**, *15*, 1–57. [CrossRef]
13. Ellenberg, H. Zeigerwerte Der Gefäßpflanzen Mitteleuropas (Indicator Values of Vascular Plants in Central Europe). *Scr. Geobot.* **1974**, *9*, 1–97.
14. Didukh, Y.P. *The Ecological Scales for the Species of Ukrainian Flora and Their Use in Synphytoindication*; Phytosociocenter: Kyiv, Ukraine, 2011.
15. Zhukov, O.; Kunakh, O. The Asymmetry of the Aquatic Macrophyte Response to Temperature Increases with Global Warming and Has to Be Accounted for in Phytoindication. *Biologia* **2025**, *80*, 529–547. [CrossRef]
16. Thornthwaite, C.W. An Approach toward a Rational Classification of Climate. *Geogr. Rev.* **1948**, *38*, 55. [CrossRef] [PubMed]
17. Diekmann, M. Species Indicator Values as an Important Tool in Applied Plant Ecology—A Review. *Basic Appl. Ecol.* **2003**, *4*, 493–506. [CrossRef]
18. Rösch, H.; Van Rooyen, M.W.; Theron, G.K. Predicting Competitive Interactions between Pioneer Plant Species by Using Plant Traits. *J. Veg. Sci.* **1997**, *8*, 489–494. [CrossRef]
19. Vicente-Serrano, S.M.; Beguería, S.; López-Moreno, J.I. A Multiscalar Drought Index Sensitive to Global Warming: The Standardized Precipitation Evapotranspiration Index. *J. Clim.* **2010**, *23*, 1696–1718. [CrossRef]
20. Schaffers, A.P.; Sýkora, K.V. Reliability of Ellenberg Indicator Values for Moisture, Nitrogen and Soil Reaction: A Comparison with Field Measurements. *J. Veg. Sci.* **2000**, *11*, 225–244. [CrossRef]
21. Tichý, L.; Axmanová, I.; Dengler, J.; Guarino, R.; Jansen, F.; Midolo, G.; Nobis, M.P.; Van Meerbeek, K.; Aćić, S.; Attorre, F.; et al. Ellenberg-type Indicator Values for European Vascular Plant Species. *J. Veg. Sci.* **2023**, *34*, e13168. [CrossRef]
22. Tutova, H.; Lisovets, O.; Kunakh, O.; Zhukov, O. From Species Traits to Community Gradients: Validation of Borhi-Di-like Naturalness Indicators in Steppe Vegetation. *Biosyst. Divers.* **2026**, *34*, e2608. [CrossRef]
23. Tutova, H.; Lisovets, O.; Kunakh, O.; Zhukov, O. Phytoindication Is a Useful Tool for Assessing the Response of Plant Communities to Environmental Factors. *Diversity* **2025**, *17*, 738. [CrossRef]
24. Kopecký, M.; Hederová, L.; Macek, M.; Klinerová, T.; Wild, J. Forest Plant Indicator Values for Moisture Reflect Atmospheric Vapour Pressure Deficit Rather than Soil Water Content. *New Phytol.* **2024**, *244*, 1801–1811. [CrossRef]
25. Hill, M.O.; Roy, D.B.; Mountford, J.O.; Bunce, R.G.H. *Ellenberg's Indicator Values for British Plants*; Institute of Terrestrial Ecology: Huntingdon, UK, 1999.
26. Ertsen, A.C.D.; Alkemade, J.R.M.; Wassen, M.J. Calibrating Ellenberg Indicator Values for Moisture, Acidity, Nutrient Availability and Salinity in the Netherlands. *Plant Ecol.* **1998**, *135*, 113–124. [CrossRef]
27. Sun, Y.; Sun, Y.; Yao, S.; Akram, M.A.; Hu, W.; Dong, L.; Li, H.; Wei, M.; Gong, H.; Xie, S.; et al. Impact of Climate Change on Plant Species Richness across Drylands in China: From Past to Present and into the Future. *Ecol. Indic.* **2021**, *132*, 108288. [CrossRef]
28. Dwyer, C.; Millett, J.; Pakeman, R.J.; Jones, L. Environmental Modifiers of the Relationship between Water Table Depth and Ellenberg's Indicator of Soil Moisture. *Ecol. Indic.* **2021**, *132*, 108320. [CrossRef]
29. Schmidtlein, S.; Ewald, J. Landscape Patterns of Indicator Plants for Soil Acidity in the Bavarian Alps. *J. Biogeogr.* **2003**, *30*, 1493–1503. [CrossRef]
30. Hájek, M.; Roleček, J.; Cottenie, K.; Kintrová, K.; Horsák, M.; Poulíčková, A.; Hájková, P.; Fránková, M.; Dítě, D. Environmental and Spatial Controls of Biotic Assemblages in a Discrete Semi-Terrestrial Habitat: Comparison of Organisms with Different Dispersal Abilities Sampled in the Same Plots. *J. Biogeogr.* **2011**, *38*, 1683–1693. [CrossRef]
31. Wamelink, G.W.W.; Joosten, V.; van Dobben, H.F.; Berendse, F. Validity of Ellenberg Indicator Values Judged from Physico-chemical Field Measurements. *J. Veg. Sci.* **2002**, *13*, 269–278. [CrossRef]

32. Raduła, M.W.; Szymura, T.H.; Szymura, M. Topographic Wetness Index Explains Soil Moisture Better than Bioindication with Ellenberg's Indicator Values. *Ecol. Indic.* **2018**, *85*, 172–179. [CrossRef]
33. Möckel, T.; Löfgren, O.; Prentice, H.C.; Eklundh, L.; Hall, K. Airborne Hyperspectral Data Predict Ellenberg Indicator Values for Nutrient and Moisture Availability in Dry Grazed Grasslands within a Local Agricultural Landscape. *Ecol. Indic.* **2016**, *66*, 503–516. [CrossRef]
34. Di Biase, L.; Tsafack, N.; Pace, L.; Fattorini, S. Ellenberg Indicator Values Disclose Complex Environmental Filtering Processes in Plant Communities along an Elevational Gradient. *Biology* **2023**, *12*, 161. [CrossRef]
35. Schmidtlein, S. Imaging Spectroscopy as a Tool for Mapping Ellenberg Indicator Values. *J. Appl. Ecol.* **2005**, *42*, 966–974. [CrossRef]
36. Dengler, J.; Jansen, F.; Chusova, O.; Hüllbusch, E.; Nobis, M.P.; Van Meerbeek, K.; Axmanová, I.; Bruun, H.H.; Chytrý, M.; Guarino, R.; et al. Ecological Indicator Values for Europe (EIVE) 1.0. *Veg. Classif. Surv.* **2023**, *4*, 7–29. [CrossRef]
37. Berg, C.; Welk, E.; Jäger, E.J. Revising Ellenberg's Indicator Values for Continentality Based on Global Vascular Plant Species Distribution. *Appl. Veg. Sci.* **2017**, *20*, 482–493. [CrossRef]
38. Coquery, T.; Welk, E.; Korell, L. Spatial Bias in GBIF Data Has Limited Impact on Plant Climate Niche Properties in Europe. *bioRxiv* **2026**, 1–32. [CrossRef]
39. Western, A.W.; Grayson, R.B.; Blöschl, G. Scaling of Soil Moisture: A Hydrologic Perspective. *Annu. Rev. Earth Planet. Sci.* **2002**, *30*, 149–180. [CrossRef]
40. Pichura, V.; Potravka, L. Impact of War on Natural and Climatic Transformation of Territories in the Irrigation Zone of Ukraine. *Discov. Appl. Sci.* **2025**, *7*, 783. [CrossRef]
41. Pichura, V.; Potravka, L.; Boiko, P. Climatic and Hydrological Conditions for the Formation of Vegetation Cover in the Drained Kakhovka Reservoir's Territory. *Ecol. Eng. Environ. Technol.* **2025**, *26*, 357–373. [CrossRef]
42. Pichura, V.; Potravka, L.A.; Domaratskiy, Y.; Nikonchuk, N.; Samoilenko, M. The Impact of Pre-Crops on the Formation of Water Balance in Winter Wheat Agrocenosis and Soil Moisture in the Steppe Zone. *J. Ecol. Eng.* **2024**, *25*, 253–271. [CrossRef]
43. Tutova, G.F.; Kunakh, O.M.; Yakovenko, V.M.; Zhukov, O.V. The Importance of Relief for Explaining the Diversity of the Floodplain and Terrace Soil Cover in the Dnipro River Valley: The Case of the Protected Area within the Dnipro-Orylskiy Nature Reserve. *Biosyst. Divers.* **2023**, *31*, 177–190. [CrossRef]
44. Mykhailyuk, T.; Lisovets, O.; Tutova, H. The Importance of Terrain Factors in the Spatial Variability of Plant Cover Diversity in a Steppe Gully. *Biosyst. Divers.* **2023**, *31*, 470–483. [CrossRef]
45. Buzhdygan, O.; Baldauf, S.; Borovyk, D.; Vynokurov, D.; Ladouceur, E.; Chusova, O.; Iemelianova, S.; Budzhak, V.; Tietjen, B.; Bezrodnova, O.; et al. Scale-Dependent Effects of Plant Diversity Drivers Across Different Grassland Habitats in Ukraine. *Ecol. Evol.* **2025**, *15*, e70941. [CrossRef]
46. Borovyk, D.; Dembicz, I.; Dengler, J.; Guarino, R.; Kuzemko, A.; Lavrinenko, K.; Moysiyenko, I.; Skobel, N.; Bednarska, I.; Babytskiy, A.; et al. Plant Species Richness Records in Ukrainian Steppes. *Tuexenia* **2024**, *44*, 225–239. [CrossRef]
47. Vynokurov, D.; Borovyk, D.; Chusova, O.; Davydova, A.; Davydov, D.; Danihelka, J.; Dembicz, I.; Iemelianova, S.; Kolomiiets, G.; Moysiyenko, I.; et al. Ukrainian Plant Trait Database: UkrTrait v. 1.0. *Biodivers. Data J.* **2024**, *12*, e118128. [CrossRef]
48. Tarasov, V.V. *Flora of Dnipropetrovsk and Zaporizhia Regions*; Travleev, A.P., Ed.; Lira: Dnipropetrovsk, Ukraine, 2012.
49. GBIF.org. European Occurrence Records of Vascular Plant Species Filtered for Ecological Analysis. *Deriv. Dataset GBIF* **2026**. [CrossRef]
50. Tutova, H.; Lisovets, O.; Kunakh, O.; Zhukov, O. European GBIF Occurrence Records of Vascular Plant Species from the Regional Flora of Dnipropetrovsk and Zaporizhzhia Regions, Ukraine. Zenodo. 2026. Available online: https://zenodo.org/records/20829434 (accessed on 25 June 2026).
51. Chamberlain, S.; Barve, V.; Mcglinn, D.; Oldoni, D.; Desmet, P.; Geffert, L.; Ram, K. *R Package*, version 3.7.9; rgbif: Interface to the Global Biodiversity Information Facility API; R Foundation for Statistical Computing: Vienna, Austria, 2024. Available online: https://CRAN.R-project.org/package=rgbif (accessed on 25 June 2026).
52. Beven, K.J.; Kirkby, M.J. A Physically Based, Variable Contributing Area Model of Basin Hydrology. *Hydrol. Sci. Bull.* **1979**, *24*, 43–69. [CrossRef]
53. Ho, Y.; Hengl, T. Multiscale Land Surface Parameters of GEDTM30: Topographic Wetness Index (Version V20241230) [Data Set]. Zenodo. 2025. Available online: https://zenodo.org/records/14920387 (accessed on 25 June 2026).
54. Fick, S.E.; Hijmans, R.J. WorldClim 2: New 1-Km Spatial Resolution Climate Surfaces for Global Land Areas. *Int. J. Climatol.* **2017**, *37*, 4302–4315. [CrossRef]
55. Hijmans, R.J.; Barbosa, M.; Ghosh, A.; Mandel, A. Geodata: Download Geographic Data. R Package Version 0.6-2. 2024. Available online: https://github.com/rspatial/geodata (accessed on 25 June 2026).
56. Poggio, L.; de Sousa, L.M.; Batjes, N.H.; Heuvelink, G.B.M.; Kempen, B.; Ribeiro, E.; Rossiter, D. SoilGrids 2.0: Producing Soil Information for the Globe with Quantified Spatial Uncertainty. *Soil* **2021**, *7*, 217–240. [CrossRef]
57. Legendre, P.; Legendre, L. Canonical Analysis. *Dev. Environ. Model.* **2012**, *24*, 625–710. [CrossRef]

58. Calatayud, J.; Neuman, M.; Rojas, A.; Eriksson, A.; Rosvall, M. Regularities in Species' Niches Reveal the World's Climate Regions. *eLife* **2021**, *10*, e58397. [CrossRef]
59. Castellanos, A.A.; Huntley, J.W.; Voelker, G.; Lawing, A.M. Environmental Filtering Improves Ecological Niche Models across Multiple Scales. *Methods Ecol. Evol.* **2019**, *10*, 481–492. [CrossRef]
60. Greenacre, M. The Contributions of Rare Objects in Correspondence Analysis. *Ecology* **2013**, *94*, 241–249. [CrossRef]
61. Clarke, K.; Chapman, M.; Somerfield, P.; Needham, H. Dispersion-Based Weighting of Species Counts in Assemblage Analyses. *Mar. Ecol. Prog. Ser.* **2006**, *320*, 11–27. [CrossRef]
62. Legendre, P.; Gallagher, E.D. Ecologically Meaningful Transformations for Ordination of Species Data. *Oecologia* **2001**, *129*, 271–280. [CrossRef]
63. Peres-Neto, P.R.; Jackson, D.A. How Well Do Multivariate Data Sets Match? The Advantages of a Procrustean Superimposition Approach over the Mantel Test. *Oecologia* **2001**, *129*, 169–178. [CrossRef]
64. Broennimann, O.; Fitzpatrick, M.C.; Pearman, P.B.; Petitpierre, B.; Pellissier, L.; Yoccoz, N.G.; Thuiller, W.; Fortin, M.; Randin, C.; Zimmermann, N.E.; et al. Measuring Ecological Niche Overlap from Occurrence and Spatial Environmental Data. *Glob. Ecol. Biogeogr.* **2012**, *21*, 481–497. [CrossRef]
65. Basille, M.; Calenge, C.; Marboutin, É.; Andersen, R.; Gaillard, J.-M. Assessing Habitat Selection Using Multivariate Statistics: Some Refinements of the Ecological-Niche Factor Analysis. *Ecol. Model.* **2008**, *211*, 233–240. [CrossRef]
66. Lessa, D.; Morard, R.; Jonkers, L.; Venancio, I.M.; Reuter, R.; Baumeister, A.; Albuquerque, A.L.; Kucera, M. Distribution of Planktonic Foraminifera in the Subtropical South Atlantic: Depth Hierarchy of Controlling Factors. *Biogeosciences* **2020**, *17*, 4313–4342. [CrossRef]
67. Aiello-Lammens, M.E.; Boria, R.A.; Radosavljevic, A.; Vilela, B.; Anderson, R.P. SpThin: An R Package for Spatial Thinning of Species Occurrence Records for Use in Ecological Niche Models. *Ecography* **2015**, *38*, 541–545. [CrossRef]
68. Boria, R.A.; Olson, L.E.; Goodman, S.M.; Anderson, R.P. Spatial Filtering to Reduce Sampling Bias Can Improve the Performance of Ecological Niche Models. *Ecol. Model.* **2014**, *275*, 73–77. [CrossRef]
69. Tutova, H.; Lisovets, O.; Kunakh, O.; Zhukov, O. Ecological Characteristics of Vascular Plants of the Dnipropetrovsk and Zaporizhzhia Regions (Ukraine): Ellenberg, Didukh, Edaphic, and Topographic Moisture Indicators. Zenodo. 2026. Available online: https://zenodo.org/records/20962053 (accessed on 25 June 2026).
70. Tutova, H.; Lisovets, O.; Kunakh, O.; Zhukov, O. Vegetation Relevé Dataset from the Ukrainian Steppe Zone for Ecological Indicator Validation [Dataset]. Zenodo. 2026. Available online: https://zenodo.org/records/21720925 (accessed on 25 June 2026).
71. Oksanen, J.; Blanchet, F.G.; Kindt, R.; Legendre, P.; Minchin, P.R.; O'Hara, R.B.; Simpson, G.L.; Solymos, P.; Stevens, M.H.H.; Wagner, H. *R Package*, version 2.5-2; Community Ecology Package; R Foundation for Statistical Computing: Vienna, Austria, 2018. Available online: https://CRAN.R-project.org/package=vegan (accessed on 25 June 2026).
72. Tutova, H.; Lisovets, O.; Kunakh, O.; Zhukov, O. Habitat Classification of the Khortytsia Island Floodplain after the Kahovka Catastrophe Using the European Nature Information System (EUNIS). *Biosyst. Divers.* **2026**, *34*, e2606. [CrossRef]
73. Lisovets, O.; Tutova, H.; Kunakh, O.; Zhukov, O. *Plant Survey Data from Khortytsia Island (Ukraine), 2025*; Occurrence Dataset; Bohdan Khmelnytsky Melitopol State Pedagogical University: Melitopol, Ukraine, 2025. [CrossRef]
74. Lindsay, J.B. Whitebox GAT: A Case Study in Geomorphometric Analysis. *Comput. Geosci.* **2016**, *95*, 75–84. [CrossRef]
75. Gao, B. NDWI—A Normalized Difference Water Index for Remote Sensing of Vegetation Liquid Water from Space. *Remote Sens. Environ.* **1996**, *58*, 257–266. [CrossRef]
76. Tutova, H.; Lisovets, O.; Kunakh, O.; Zhukov, O. Temporal Matching of Unsupervised Cluster Structures for Monitoring Post-Catastrophic Floodplain Dynamics: A Case Study of Khortytsia Island. *Land* **2026**, *15*, 624. [CrossRef]
77. Tutova, H.; Lisovets, O.; Kunakh, O.; Zhukov, O. Comparison of Methods for Temporal Correspondence of Spectral Clusters: A Case Study of Post-Catastrophic Landscape Dynamics. *Geographies* **2026**, *6*, 70. [CrossRef]
78. Ulrich, W. Species Co-Occurrences and Neutral Models: Reassessing J. M. Diamond's Assembly Rules. *Oikos* **2004**, *107*, 603–609. [CrossRef]
79. Wankmüller, F.J.P.; Delval, L.; Lehmann, P.; Baur, M.J.; Cecere, A.; Wolf, S.; Or, D.; Javaux, M.; Carminati, A. Global Influence of Soil Texture on Ecosystem Water Limitation. *Nature* **2024**, *635*, 631–638. [CrossRef]
80. Saxton, K.E.; Rawls, W.J. Soil Water Characteristic Estimates by Texture and Organic Matter for Hydrologic Solutions. *Soil Sci. Soc. Am. J.* **2006**, *70*, 1569–1578. [CrossRef]
81. Xue, S.; Wu, G. A Study of the Dependence between Soil Moisture and Precipitation in Different Ecoregions of the Northern Hemisphere. *Hydrol. Earth Syst. Sci.* **2025**, *29*, 5575–5591. [CrossRef]
82. Zignol, F.; Lidberg, W.; Greiser, C.; Larson, J.; Hoffrén, R.; Ågren, A.M. Controls on Spatial and Temporal Variability of Soil Moisture across a Heterogeneous Boreal Forest Landscape. *Hydrol. Earth Syst. Sci.* **2025**, *29*, 5493–5513. [CrossRef]
83. Winzeler, H.E.; Owens, P.R.; Read, Q.D.; Libohova, Z.; Ashworth, A.; Sauer, T. Topographic Wetness Index as a Proxy for Soil Moisture in a Hillslope Catena: Flow Algorithms and Map Generalization. *Land* **2022**, *11*, 2018. [CrossRef]

84. Coleman, M.L.; Niemann, J.D. Controls on Topographic Dependence and Temporal Instability in Catchment-scale Soil Moisture Patterns. *Water Resour. Res.* **2013**, *49*, 1625–1642. [CrossRef]
85. Khomiak, I.V.; Onyshchuk, I.P.; Vakerych, M.M.; Hasynets, Y.S.; Schwartau, V.V. Restoration of Floodplains' Natural Vegetation of Polissia to Reduce the Effects of Climate Change. *Biosyst. Divers.* **2025**, *33*, e2551. [CrossRef]
86. Minarchenko, V.; Tymchenko, I.; Pushkarova, Y.; Dvirna, T.; Futorna, O.; Polishchuk, O. Impact of Climate Change on Populations and Resources of Convallaria Majalis. *Biosyst. Divers.* **2025**, *33*, e2543. [CrossRef]
87. Chetvertak, T.; Diuzhykova, T.; Hryshko, S.; Nepsha, O.; Tutova, H. The Precipitation Levels during the Warmest Quarter Are the Primary Factor Influencing the Spatial Distribution of Opatrum Sabulosum. *Biosyst. Divers.* **2025**, *33*, e2507. [CrossRef]
88. Nykytiuk, Y.; Kravchenko, O.; Komorna, O. Bioclimatic and Soil Determinants of Buckwheat Cultivation Prospects under Global Warming: A Case Study of the Ukrainian Polissya and Forest-Steppe. *Biosyst. Divers.* **2025**, *33*, e2537. [CrossRef]
89. Nykytiuk, Y.; Kravchenko, O.; Vyskushenko, D.; Pitsil, A.; Komorna, O.; Bezvershuck, I. Bioclimatic Constraints and Edaphic Preferences of Wheat: Implications for Environmental Suitability Forecasting under Climate Change. *Stud. Biol.* **2025**, *19*, 137–156. [CrossRef]
90. Nykytiuk, Y.; Kravchenko, O. Maize Response Patterns to Soil and Climate Factors Form the Basis for Predicting Changes in Its Growing Conditions under Climate Change. *Biosyst. Divers.* **2025**, *33*, e2553. [CrossRef]
91. Zelený, D.; Schaffers, A.P. Too Good to Be True: Pitfalls of Using Mean Ellenberg Indicator Values in Vegetation Analyses. *J. Veg. Sci.* **2012**, *23*, 419–431. [CrossRef]

Disclaimer/Publisher's Note: The statements, opinions and data contained in all publications are solely those of the individual author(s) and contributor(s) and not of MDPI and/or the editor(s). MDPI and/or the editor(s) disclaim responsibility for any injury to people or property resulting from any ideas, methods, instructions or products referred to in the content.